At-a-site and between-site variability of bedload transport, inferred from continuous surrogate monitoring, and comparison to predictive equations

Dieter Rickenmann [1,2]

5   [1]Swiss Federal Research Institute WSL, Birmensdorf, 8903, Switzerland
[2]FluvialTech GmbH, Zürich, 8052, Switzerland

Correspondence to: Dieter Rickenmann (dieter.rickenmann@wsl.ch)

Abstract. This study investigates spatial and temporal variability of bedload transport in four Swiss mountain streams using continuous Swiss Plate Geophone (SPG) monitoring. This surrogate measuring system had been calibrated in previous studies

10   to produce reliable estimates of bedload transport rates. The measurements were analysed at two different time scales: short-term transport events typically covering a duration of a few weeks and multi-year annual transport totals. Power-law relations between dimensionless transport intensity and shear stress were derived to evaluate the temporal variability in the steepness of transport relations and in the reference shear stress. Results were compared with predictive equations developed for mountain streams. Findings show substantial variability both within and across sites, likely reflecting the influence of sediment

15   availability, stream slope, streambed texture and flow history. Overall, continuous monitoring highlights the strong role of temporal spatial variability on bedload transport levels, possibly due to changing sediment availability and bed surface composition, and with implications for predictive modelling and river management.

1 Introduction

Traditionally, bedload transport has been modeled using semi-empirical relations between mean transport and mean hydraulic

20   variables such as shear stress or flow discharge (Bagnold, 1966; Meyer-Peter and Müller, 1948; Recking, 2013; Schneider et al., 2015a; Wilcock and Crowe, 2003). However, extensive field measurements and flume experiments have demonstrated that bedload transport is often highly variable at multiple spatial and temporal scales. Many reasons for the variability were listed by Ancey (2020), and they include the mixing of fast and slow processes, nonequilibrium and noise-driven processes, cascades of interacting processes, varying temporal and spatial scales dependent on flow conditions, heterogeneity of materials and flow

25   conditions, nonlinearity and threshold effects, and poor knowledge of initial and boundary conditions.

One of the most important elements of variability is the threshold of motion. The Shields number (e.g., Buffington and Montgomery, 1997) describes a critical dimensionless shear stress for particle entrainment. However, observations have shown that individual grains move both below and above the predicted threshold due to turbulence, grain protrusion, and intergranular force chains (Nelson et al., 1995; Diplas et al., 2008). Particle motion reflects stochastic impulses, resulting in intermittent

Type text here

30   entrainment. Laboratory studies confirm that impulse duration and magnitude are more predictive than mean shear stress (Valyrakis et al., 2010).

Memory effects or history dependence can affect bedload transport variability. For example, the threshold for motion is influenced by factors such as flow duration, prior high or low flows, and disturbance of the bed (by floods or large transport events). In low-flow or inter-event periods, the bed surface stabilizes (settlement, compaction), thereby increasing the

35   entrainment threshold, observed both in flume experiments and for example in the Swiss Erlenbach stream (Masteller and Finnegan, 2017; Masteller et al., 2019). Conversely, at higher flows with important sediment supply to and deposition on the channel, observations at the Erlenbach showed a decrease of the entrainment threshold (Rickenmann, 2020, 2024). In mixed-size sediments, bed-surface structure produces partial transport, whereby only a fraction of the surface is mobile at a given flow (Wilcock and McArdell, 1993; Parker, 2008). Surface armoring shields finer grains and creates patchy mobility, while

40   coarser clasts may move only episodically during high flows (Church, 2006; Turowski et al., 2009; Vázquez-Tarrío et al., 2020). This selective mobility introduces large variability into fractional bedload rates. Bed shear stress is not spatially uniform but dominated by coherent turbulent structures. Bursts, sweeps, and vortices impart localized impulses capable of mobilizing grains otherwise at rest (Nelson et al., 1995; Schmeeckle and Nelson, 2003; Dwivedi et al., 2010).

Evolving bedforms and morphological structures (e.g., ripples, dunes, alternate bars, step-pool structures) contribute to

45   temporal and spatial variability by alternately storing and releasing sediment (Vázquez-Tarrío et al., 2020). Migrating bedforms and structures impose oscillations in transport at timescales linked to bedform wavelength and celerity (Gomez et al., 1989) and to strong flow events capable of destroying step-pool structures (Golly et al., 2017). Bed topography also generates localized roughness, further amplifying spatial heterogeneity in transport rates (Monsalve et al., 2020). Phase-1 bedload transport typically involves finer grains and is controlled more by upstream sediment supply and availability than by water

50   discharge; in contrast, phase-2 bedload transport shows a clear dependence on water discharge, and particles from the bed surface layer are also likely to be mobilized (Church, 2010; Rickenmann, 2018; Warburton, 1992).

Bedload variability also reflects external forcings such as landslides, debris flows, and tributary inputs. Such pulses of material supply can temporarily overwhelm the transport capacity, creating surges of bedload independent of discharge (Lisle et al., 1997). Experimental evidence shows that episodic sediment supply increases variability, especially at longer timescales

55   (Elgueta-Astaburuaga and Hassan, 2018). Hydrograph dynamics further amplify variability: transport often peaks disproportionately on the rising limb relative to falling stages due to supply exhaustion and channel adjustments (Pretzlav et al., 2020; Mao et al., 2019; Rickenmann, 2024).

Recking et al. (2016) compiled bedload transport measurements from more than 100 streams with the goal to study how river bed morphology (such as step-pool, riffle-pool, braiding, plane beds, sand beds) influences fluvial bedload transport rates.

60   They used a standard bedload transport equation as a function of shear stress as a reference situation, whereby this equation (Recking, 2013) was developed in such a way that it can be linked to bedload measured in narrow flumes in the absence of any bed form. They applied a generalized form of the equation to the many streams, varying either the exponent (steepness) of the bedload transport relation for the steep part of the equation or the reference shear stress, to find a good agreement of the

65   predictions with the measurements. Both the steepness and the reference shear stress have generally a large effect on the predicted bedload transport level, and the study found that both optimized variables varied in a considerable range. Furthermore, Recking et al. (2016) showed that the optimal steepness (exponent) varied somewhat with channel geometry and bedform type, and that the optimal reference shear stress strongly depended on channel slope. They concluded that only narrow natural channels, especially those with plane beds, behave like a flume, while larger rivers deviate more from the flat-bed flume situation. For riffle-pool morphologies, they further found a grain-size distribution effect, likely a proxy for the riffle-

70   pool development, on the optimal reference shear stress.

Until about two decades ago, direct bedload measurements were the main means to quantify its variability in natural streams. However, most of these measurements suffered from the important limitation that typically only discrete samples were taken in time and space (in a given cross-section), and sampling at higher flows was often not feasible. After about 2005, more and more surrogate bedload systems with impact plate geophones were installed in gravel-bed streams (Coviello et al., 2022;

75   Rickenmann, 2017; Rickenmann et al., 2022; Rindler et al., 2025). These indirect measurements have the advantage of a continuous monitoring of bedload transport, typically using a one-minute recording interval, and of including also higher flows.

Rickenmann (2018) analyzed measurements with Swiss plate geophones (SPG) from six years in the two glacier-fed mountain streams Fischbach and Ruetz in Austria. He observed that an exponential form of the Meyer-Peter and Mueller (MPM) equation

80   (Cheng, 2002) could reasonably well represent the increase in bedload transport with discharge for phase-2 transport conditions. A back-calculation of appropriate Shields numbers (which are similar to dimensionless reference shear stresses for the exponential MPM form) showed seasonal and year-to-year fluctuations, with the Shield values mostly ranging from 0.01 to 0.06. In these calculations, an effective or reduced shear stress was used together with the exponential MPM equation. In the same study, Rickenmann (2018) found that correlation between bedload transport rates and discharge is considerably

85   increased, if these values are aggregated over about one to two hours. Observations from the Erlenbach stream with the SPG system showed that disequilibrium ratio of measured to calculated transport values influenced bedload transport behavior (Rickenmann, 2020, 2024). Above-average disequilibrium conditions, which were associated with a greater sediment availability on the streambed, generally had a stronger effect on subsequent transport conditions than below-average disequilibrium conditions, which were associated with comparatively less sediment availability on the streambed.

90   Coviello et al. (2022) also used an impact plate geophone system and considered longer-term fluctuations of bedload transport. They analyzed seven years of bedload data in the glacier-fed Italian Sulden stream and found that climatic factors (snow cover and temperature) modulate bedload flux seasonally and inter-annually. They also found that, for the same discharge in different seasons, transport rates can differ markedly. Kreisler et al. (2017) measured bedload transport with impact plate geophones at the Urslau torrent in Salzburg. They analyzed three years of data including more than 30 individual bedload-transporting flood

95   events and found that bedload transport efficiency, defined as the ratio of observed bedload transport to excess stream power, varied considerably among different events and across years. Their study also showed that variable sediment supply conditions affected the prevailing bedload transport rates at the Urslau stream. Aigner et al. (2017) used impact plate geophone

measurements over a 15-year period in the Upper Drau River in Austria, obtained from instruments installed 2 km downstream

of a reach with only residual flow, due to the existence of an upstream hydropower plant. Their analysis revealed a complex

100 process of gravel storage and intermittent re-supply from the residual upstream reach. Frequently occurring bedload pulses

produced very high bedload fluxes while in transit and tended to increase bedload flux in the post-event phase, and could alter

and reduce the sediment storage in upstream reaches, leading to a reduction in bedload availability for future pulses.

The goal of this study is to quantify the variability of bedload transport in detail in four mountain streams in Switzerland, as

inferred from continuous measurements with the SPG system, for two different time scales. The first analysis addresses the

105 temporal variability of bedload transport for a given year, where active periods of bedload movement typically occurred in the

summer half-year in the four streams. The variability is quantified by determining power law relations between transport rates

and shear stresses, for the steep part of the transport relations (phase-2 transport conditions), and typically over successive

two-weeks periods. The resulting power law equations allow to determine the steepness of the bedload rating curve and to

infer a corresponding reference shear stress. This analysis permits a comparison and discussion with the comprehensive study

110 of Recking et al. (2016) that considered the between-site variability of the same two variables (steepness and reference shear

stress) for a large data set including direct bedload measurements, mentioned above. The second analysis aims to compare

calculated and observed bedload masses summed up over individual years, considering extended data sets for the same four

Swiss streams with typical observation durations of several years.

2 Observation sites, bedload transport equations and analysis

115 2.1 Observation sites, SPG calibration, and discharge data

Measurements with the SPG System have been obtained in five Swiss mountain streams over several years (e.g. Rickenmann

et al., 2022; Schneider et al., 2016; and further references in Table 1). Here I first compare one-year measurements from these

five streams (Table 1) with four bedload transport equations. The main stream characteristics necessary for the bedload

transport calculations are also listed in Table 1. For all of these streams, calibration relations were already discussed in

120 Antoniazza et al. (2022), Rickenmann et al. (2012), Nicollier et al. (2021,2022), and Schneider et al., (2016). The location of

the five SPG sites is shown in Fig. 1. For the further analysis as described in section 2.3 and 2.4, only four streams were

considered, the Riedbach was excluded due to the limited time resolution of the SPG data.

Table 1. Characteristics of Swiss field sites with SPG measurements. A_c = catchment area, Q_{max} = maximum discharge

for the observation year, w = channel width, S = channel slope, D_{xx} = characteristic grain size (see also text and Appendix

B).

SPG site	A_c (km^2)	Q_{max} (m^3/s)	w (m)	S (%)	D_{84} (m)	D_{50} (m)	References
Albula	529	96	14	0.7	0.16	0.065	[1], [2], [3], [4], [5]

Navisence	47.0	31	13	2.8	0.23	0.10	[4], [5], [6]
Avançon	13.4	6.4	5.8	4.0	0.36	0.06	[7], [8], [9]
Erlenbach	0.74	15	4.1	10.5	0.29	0.06	[9], [10], [11], [12], [13]
Riedbach	15.8	4.5	4.0	38.0	0.91	0.38	[14], [15]

[1] Rickenmann et al. (2017), [2] Nicollier et al. (2019), [3] Rickenmann et al. (2020),

[4] Nicollier et al. (2021), [5] Nicollier et al. (2022), [6] Nicollier et al. (2020),

[7] Antoniazza et al. (2022), [8] Antoniazza et al. (2023), [9] Rickenmann et al. (2022),

[10] Rickenmann and McArdell (2007), [11] Rickenmann et al. (2012), [12] Rickenmann et al. (2020), [13] Rickenmann et al. (2024), [14] Schneider et al. (2015b), [15] Schneider et al. (2016)
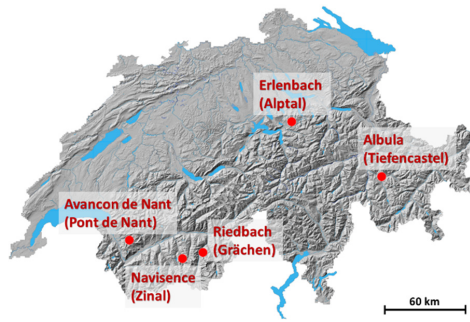
Figure 1. Field sites in Swiss streams with SPG measurements.

125

The SPG System recorded summary values including impulses (IMP) for one-minute intervals at the first four sites in Table 1, whereas IMP values were stored only for 10-minute intervals for the Riedbach stream. For this study, new calibration relations were defined for the three streams, namely for the Albula, the Navisence, and the Avançon, according to the following equation:

130
$$M = k_{site}\, IMP \tag{1}$$

For the calibration, M = measured bedload mass (in kg, for grain size $D > 9.5$ mm), k_{site} = linear calibration coefficient with the units (kg), and IMP = sum of impulses recorded over one-minute intervals. These calibration coefficients were reported in Baldig and Rickenmann (2024). For the Erlenbach, the linear calibration coefficient varied according to the survey periods of the deposited sediments in the retention basin (Rickenmann, 2020, 2022), and for the Riedbach a power-law calibration relation

135 was determined (Schneider et al., 2016). The calibration coefficients and equations used in this study for the different SPG sites are summarized in Table 2. The measured bedload transport rate Q_b (in kg s-1) was derived by dividing the transported bedload mass by the respective recoding time interval in seconds, and it represents the total bedload discharge over the entire stream width.

Table 2. Calibration coefficients and equations used for the different SPG sites. The calibration coefficient k-isp for the Erlenbach refers to individual survey periods of the sediment deposits in the retention basin. (*) A power law calibration equation was used for the Riedbach.

Site	k_{site}	n	R2	References
Albula	0.0873	51	0.?24	Baldig & Rickenmann (2024)
Navisence	0.0720	51	0.590	Baldig & Rickenmann (2024)
Avançon	0.0792	55	0.729	Baldig & Rickenmann (2024)
Erlenbach	k-isp	NA	NA	Rickenmann (2020, 2024)
Riedbach	(*)	15	0.992	Schneider et al. (2016)

140

Observations of bedload transport often show a large variability for a given discharge value, typically covering several orders of magnitudes. In such a situation, when binning the measurements into discharge classes to determine a mean trend of the observed transport rates, it is preferable to calculate the geometric mean of the Q_b values. However, this brings about the problem of how to deal with observed zero Q_b values. Here, I took an approach similar to that proposed by Gaeuman et al.

145 (2009, 2015), averaging the zero $Q_b = Q_{bz}$ values with (temporally) neighboring non-zero Q_b values. I replaced the Q_{bz} values by averaging any k successive Q_{bz} values by including the two neighboring non-zero Q_{bz_p} and Q_{bz_a} values, where the indices stand for p=prior and a=after a series of k successive Q_{bz} values. Then I assigned to all $(k+2)$ values the average value $Q_{bM} = (Q_{bz\_p} + Q_{bz\_a})/(k+2)$. This procedure was previously applied to the Erlenbach bedload measurements (Rickenmann, 2024). Thus, contrary to the Q_b values that include zero values, all the Q_{bM} values are non-zero and a representative geometric mean

150 value can be calculated for a given discharge class.

At four sites (Navisence, Avançon, Erlenbach, and Riedbach) discharge measurements of Q (in $m^3 s^{-1}$) were available at the location of the SPG measurements (see references in Table 1). At the Albula river in Tiefencastel runoff gauging station is located a few hundred meters downstream of the SPG site. These discharge data were corrected for bypassed water used by a hydropower company and returned to the river in the reach in-between the two sites (Rickenmann et al., 2017).

155 **2.2 Flow resistance calculations and bedload transport equations**

The flow-resistance and the bedload-transport calculations were made four all five streams as described in Rickenmann (2020, 2022) for the Erlenbach. They were based on the measured trapezoidal cross-section in the natural reach upstream of the SPG measuring installations. Characteristic grain sizes D_{xx}, channel bottom width w, and channel slope S are given in Table 1; D_{xx} is the grain size for which xx % of the particles by mass are finer. The flow-resistance calculations were made with a hydraulic

160 geometry flow resistance relation developed by Rickenmann and Recking (2011), and they are summarized in Appendix A. Similar as for the Erlenbach (Rickenmann, 2020, 2024), the bedload-transport calculations were performed using two equations reported in Schneider et al. (2015a), which represent a modified form of the Wilcock and Crowe (2003) equation and predict

total bedload transport rates (not fractional transport rates) for grain sizes larger than 4 mm. The first one (SEA1) is based on the use of total shear stress and a slope-dependent reference shear stress:

$$165 \quad W_{tot}^* = 0.002 \left(\frac{\tau_{D50}^*}{\tau_{rD50}^*} \right)^{16.1} \qquad for \ \frac{\tau_{D50}^*}{\tau_{rD50}^*} < 1.143 \ and \ D > 4 \ mm \tag{2a}$$

$$W_{tot}^* = 14 \left(1 - \frac{0.85}{(\tau_{D50}^*/\tau_{rD50}^*)^{0.7}} \right)^{4.5} \qquad for \ \frac{\tau_{D50}^*}{\tau_{rD50}^*} \geq 1.143 \ and \ D > 4 \ mm \tag{2b}$$

where the dimensionless transport rate W^*_{tot} according to Wilcock and Crowe (2003) is defined as:

$$W_{tot}^* = (s-1)gqb/u^{*3} \tag{3}$$

and where $s = \rho_s/\rho$ = relative sediment density, with ρ_s = sediment particle density and ρ = water density, q_b = volumetric

170 bedload transport rate per unit width, $u^* = (\tau/\rho)^{0.5}$ = shear velocity, and $\tau = g\rho rhS$ = bed shear stress. $\tau^*_{D50} = rhS/(RD_{50})$ is the dimensionless bed shear stress with regard to the characteristic grain size D_{50}, and τ^*_{rD50} is the dimensionless reference bed shear stress with regard to the characteristic grain size D_{50} of the bed surface. The threshold between low and high intensity transport in Eq. (2) has been corrected to $\tau^*_{D50}/\tau^*_{rD50} = 1.143$ (Rickenmann, 2024), as compared to the value of 1.2 given in Schneider et al. (2015a). τ^*_{rD50} is calculated as a function of the bed slope (Schneider et al., 2015a, Eq. 10 therein):

$$175 \quad \tau_{rD50}^* = 0.56 \, S^{0.5} \tag{4}$$

The bedload transport rate over the entire channel width Q_b (in kg s-1), calculated with the total shear stress, is given as:

$$Q_{btot} = w \, \rho_s \, W_{tot}^* \, u^{*3} \, /((s-1)g) \tag{5}$$

The second equation (SEA2) is based on a reduced (effective) shear stress τ', using a reduced energy slope S' (Rickenmann and Recking, 2011; Schneider et al., 2015a):

$$180 \quad \tau' = g \, \rho \, r_h \, S' \tag{6}$$

$$S' = S \, (f_o \, / f_{tot}) S^{0.5 \, e} \tag{7}$$

where e = 1.5, f_{tot} = friction factor for total flow resistance, calculated with Eq. (A1), and f_o = friction factor associated with grain resistance, calculated as (Rickenmann and Recking, 2011):

$$f_o = (8 \, /6.5^2) \, (D_{84} \, /r_h)^{0.334} \tag{8}$$

185 The dimensionless transport rate W^*_{red} is determined as:

$$W_{red}^* = 0.002 \left(\frac{\tau_{D50}^{*\prime}}{\tau_{rD50}^{*\prime}} \right)^{7.8} \qquad for \ \frac{\tau_{D50}^{*\prime}}{\tau_{rD50}^{*\prime}} < 1.33 \ and \ D > 4 \ mm \tag{9a}$$

$$W_{red}^* = 14 \left(1 - \frac{0.894}{(\tau_{D50}^{*\prime}/\tau_{rD50}^{*\prime})^{0.5}} \right)^{4.5} \qquad for \ \frac{\tau_{D50}^{*\prime}}{\tau_{rD50}^{*\prime}} \geq 1.33 \ and \ D > 4 \ mm \tag{9b}$$

For equation (SEA2) the slope-independent dimensionless reference shear stress is constant:

$$\tau_{rD50}^{*\prime} = 0.03 \tag{10}$$

190 The bedload transport rate over the entire channel width Q_b, calculated with the reduced shear stress, includes the shear velocity $u^{*\prime} = (\tau'/\rho)^{0.5}$ and is given as:

$$Q_{bred} = w\,\rho_s\,W_{red}^*\,u^{*\prime 3}\,/((s-1)g) \tag{11}$$

For the development of Eq. (2) and Eq. (9), Schneider et al. (2015a) used bedload transport measurements from 14 mountain streams, including channel slopes mainly from steep streams (SS) in the range $0.01 < S < 0.11$ (except for the Oak Creek with

195   $S = 0.0014$). The bedload transport characteristics of these 14 mountain streams (called "main data set" in Schneider et al., 2015a) are labeled SEA_SS data in this study and compared with our results below. Similarly, data from 21 streams with Helley-Smith bedload samples (called "HS data set" in Schneider et al., 2015a) are labeled "SEA_HS" data in this study and compared with our results below.

Regarding possible overlap with the five streams listed in Table 1, basket samples from the Erlenbach (Rickenmann et al.,

200   2012) and net samples from the Riedbach in the flat upstream reach Schneider et al. (2015b) were used in the SEA_SS data set. However, for both two streams the SPG measurements were independent of the samples analyzed in the in the SEA_SS data set by Schneider et al. (2015a).

For further comparison with other transport equations introduced below, the steep part of the bedload transport relations (Eq. 2a, 9a) is expressed in general form as:

205   $$W^* = a\left(\frac{\tau^*}{\tau_{ref}^*}\right)^m \tag{12}$$

$$W^* = (s-1)gq_b/u^{*3} \tag{13}$$

In (12), a is a coefficient, m is an exponent, and τ^* and τ^*_{ref} may refer to calculations with either the total shear stress (Eq. 2) or with a reduced shear stress (Eq. 9).

Another bedload transport equation by Recking et al. (2016) is used here, where Φ_b is a dimensionless transport rate:

210   $$\Phi_{b84} = A\,\tau_{D84}^{*\ \alpha}\,(\tau_{D84}^*/(1 + \left(\frac{\tau_{refRe}^*}{\tau_{D84}^*}\right)^\beta)) \tag{14}$$

$$\Phi_{b84} = q_b/\sqrt{(s-1)gD_{84}^3} \tag{15}$$

$$\tau_{D84}^* = r_h\,S/((s-1)D_{84}) \tag{16}$$

where A is a coefficient, and α and β are exponents. For the general comparison with measured Q_b values of the Swiss streams, I used $A = 14$, $\alpha = 2.5$ and $\beta = 4$ (Recking, 2012, 2013) and two different equations to calculate the dimensionless reference

215   shear stress τ_{rRe}^*:

$$\tau_{rRe\_min}^* = (5\,S + 0.06)\,(D_{84}/D_{50})^{(4.4\,\sqrt{S}-1.5)} \tag{17a}$$

$$\tau_{rRe\_ss}^* = (5\,S + 0.06)\,(D_{84}/D_{50})^{(-1.5)} \tag{17b}$$

where $\tau_{rRe\_min}^*$ was recommended by Recking (2013) for calculations in streams with limited sediment availability, and $\tau_{rRe\_ss}^*$ was recommended by Recking (2012) for calculations in streams with a high sediment supply. The resulting bedload transport

220   rates over the entire channel width Q_b are then:

$$Q_{bRe\_min} = w\,\rho_s\,\Phi_{b84}\sqrt{(s-1)gD_{84}^3} \qquad \text{(for } \Phi_{b84} \text{ with } \tau^*_{rRe\_min}) \tag{18a}$$

$$Q_{bRe\_ss} = w\,\rho_s\,\Phi_{b84}\sqrt{(s-1)gD_{84}^3} \qquad \text{(for } \Phi_{b84} \text{ with } \tau^*_{rRe\_ss}) \tag{18b}$$

The steep part of Eq. (14), for τ^*_{D84} approaching zero, can be written as (Recking et al., 2016):

$$\Phi_{b84} = A\, \tau^*_{D84}{}^{\alpha+\beta} / \tau^*_{refRe}{}^{\beta} \tag{19}$$

225 Here I also compare the bedload transport equations above with the often-used equation of Meyer-Peter and Müller (1984) equation (MPM) for gravel-bed streams:

$$\Phi_b = 8\,(\tau^*_{D50} - \tau^*_c)^{1.5} \tag{20}$$

$$\Phi_b = q_b / \sqrt{(s-1)gD_{50}^3} \tag{21}$$

where τ^*_c = critical dimensionless shear stress at initiation of motion (or Shields number) with reference to D_{50}. A drawback

230 of the MPM equation and similar equations based on excess shear stress ($\tau^* - \tau^*_c$) is the use of the Shields number below which zero transport is predicted. Therefore, I use here also an exponential formulation of the MPM equation. It was first proposed by Cheng (2002), and it is given here in a slightly modified form, using a coefficient of 8 as for equation (20):

$$\Phi_b = 8\, \tau^*_{D50}{}^{1.5} exp^{(-\tau^*_c / \tau^*_{D50}{}^{1.5})} \tag{22}$$

where τ^*_c = 0.05 was given by Cheng (2002). For better comparison with dimensionless reference-shear stress (τ^*_{ref}) equations

235 presented above, I use a conversion equation from Wilcock et al. (2009), who showed that:

$$\tau^*_c = 0.996\, \tau^*_{ref} \tag{23}$$

Eq. (23) was derived by transforming Eq. (20) of MPM into a form of Eq. (12), for which the reference shear stress τ^*_{ref} is defined and determined for the following dimensionless (reference) transport rate of W^* (Wilcock et al, 2009):

$$W^*_{ref} = 0.002 \tag{24}$$

240 The dimensionless reference shear stresses used for the further calculations in this study are summarized in Table 3. Here, the two forms of the MPM equation (Eq. 20, 22) are applied only to the Albula site. The bedload transport rates over the entire channel width are labeled Q_{bMPM} for Eq. (20) and $Q_{bMPMexp}$ for Eq. (22). The aim is to illustrate how all the bedload transport equations presented above compare with each other, when applied to a given site. For the Albula site, τ^*_{refD50}= 0.0469 is used (from Eq. 4); for the traditional form of the MPM equation (20), in combination with Eq. 23, τ^*_c = 0.996 τ^*_{ref} = 0.996 τ^*_{refD50}=

245 0.0467 is used. This value is rather close to the traditional value of τ^*_c = 0.047 often used with the MPM equation. The comparison of all six bedload transport equations applied to the Albula site is shown in Fig. 2.

Table 3. Dimensionless reference shear stresses (τ^*_r) used for the calculations with the different bedload transport equations. For the application of $Q_{bMPMexp}$ to the Albula, τ^*_{ref} = 0.0467, as compared to the application of Q_{btot} to the Albula with τ^*_{rD50} = 0.0469. $Q_{1.1}$ is the water discharge corresponding to a dimensionless shear stress τ^*_{D50} = 1.1 τ^*_{rD50}. Q_c is the critical discharge for begin of substantial bedload transport, corresponding to the begin of phase-2 transport conditions.

SPG site	τ^*_{rD50}	$Q_r(\tau^*_{rD50})$	$\tau^{*'}_{rD50}$	$Q_r(\tau^{*'}_{rD50})$	$\tau^*_{rRe\_min}$	$\tau^*_{rRe\_ss}$	$Q_{1.1}(1.1\tau^*_{rD50})$ (m³ s⁻¹)	Q_c (m³ s⁻¹)

Albula	0.047	17.4	0.03	13.8	0.095	0.025	21.4	10
Navisence	0.094	15.1	0.03	7.59	0.200	0.057	18.6	2
Avancon	0.112	1.15	0.03	1.70	0.260	0.018	1.45	0.75
Erlenbach	0.181	0.524	0.03	0.501	0.585	0.055	0.661	0.5
Riedbach	0.345	10.0	0.03	4.57	1.96	0.217		
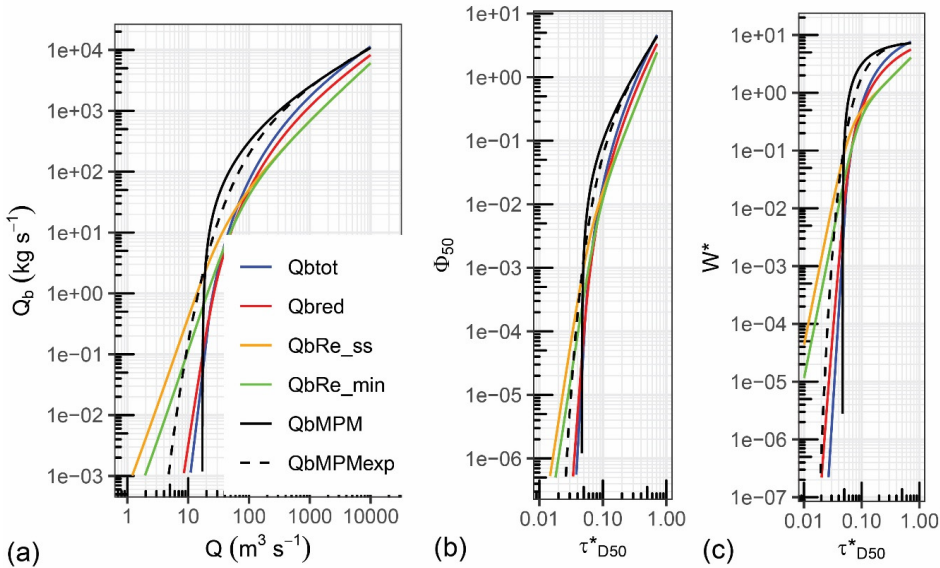
Figure 2 Bedload transport equations used and discussed in this study. To compare the six equations in one plot for each representation, they were applied here to the channel characteristics of the Albula River.

250 **2.3 Determining the steepness of bedload relations and the reference shear stress based on observed transport rates for different time windows**

Here I summarize the analysis to quantify the temporal variability of bedload transport during the active periods of bedload movement, which typically occurred in the summer half-year in the all the streams. For the Albula (2016), Navisence (2011), and Avançon (2019) streams I selected a year (given in parentheses) that included events with significant discharges and

255 bedload transport rates. For the Erlenbach, I used the two main observation periods, A (1986-1999) and B (2002-2016). Each period included a similar total duration of active bedload movement as for the first three streams (Table 4).

10

Table 4. One-year-analysis of the temporal variations. Measured and calculated bedload masses for the Swiss streams and limiting discharges Q indicating phase-2-transport conditions. Bedload masses are given here for the entire observation period and for phase-2 flow periods only.

SPG site	begin date	end date	minute values	MQ_{bM} (kg)	MQ_{btot} (kg)	MQ_{bred} (kg)	phase 2, Q range	MQ_{bM} (kg) phase 2	MQ_{btot} (kg) phase 2	MQ_{bred} (kg) phase 2
Albula	21.05.2016	21.08.2016	9.6E+04	1.1E+07	6.2E+06	4.8E+06	7 < Q < 25	3.3E+06	4.1E+05	5.0E+05
Navisence	18.05.2011	30.09.2011	1.8E+05	1.9E+06	1.2E+05	8.2E+05	3 < Q < 10	1.4E+06	3.8E+03	1.3E+05
Avancon	19.04.2019	08.11.2019	1.9E+05	4.4E+06	1.5E+07	4.2E+06	0.6 < Q < 2.0	2.5E+06	1.5E+06	1.3E+05
Erlenbach A	21.10.1986	30.09.1999	3.8E+04	6.1E+06	5.0E+06	1.5E+06	0.5 < Q < 2.0	4.6E+06	3.8E+06	8.1E+05
Erlenbach B	16.11.2002	26.10.2016	3.4E+04	8.2E+06	6.7E+06	2.8E+06	0.5 < Q < 2.0	4.5E+06	3.9E+06	8.5E+05

A closer inspection of the mean bedload transport relations over limited time periods, namely for two-week periods for the

260 first three streams, showed that these relations varied over time within an intermediate flow range including phase-2 transport conditions. For each stream the phase-2 conditions suitable for this analysis were determined by visual inspection of the smoothened trend lines. For the Erlenbach stream, flow events involving bedload transport occurred sporadically, typically lasting only about 1-2 hours. Therefore, I selected the characteristic sub-periods identified in Rickenmann (2024), namely 7 sub-periods for period A (1986-1999) and 6 sub-periods for period B (2002-2016). These sub-periods have similar

265 disequilibrium ratios. This resulted in a roughly similar total number of minute values as for the two-week periods analyzed for the other three streams. The conditions of the analyzed discharge ranges for phase-2 transport conditions for the four streams are reported in Table 4, together with other summary information on bedload transport. This includes the total bedload mass summed over the summer half-year, for the observed yearly values MQ_{bM}, as well as for the calculated yearly values using the two SEA equations (2) and (9), i.e. MQ_{btot} and MQ_{bred}.

270 Using the data for the phase-2 transport conditions only, I then determined power-law relations in the domain W^* vs. (τ^*/τ^*_{ref}) to approximate the measured bedload transport rates, resulting in one equation of the form of Eq. (12) for each two-week period (Albula, Navisence, and Avançon) or sub-period (Erlenbach). From the power-law relation fitted to the measurements, the exponent m is known, and by using the condition $W^*_{ref} = 0.002$ (Eq. 24), the dimensionless reference shear stress τ^*_{ref} was determined according to Eq. (12). This procedure was applied with both SEA equations (2) and (9), i.e. using W^*_{tot} and W^*_{red}

275 separately for all investigated data sets. The variables determined from the W^*_{tot} analysis are labeled m_{tot} and τ^*_{D50}, and those from the W^*_{red} analysis are labeled m_{red} and $\tau^*'_{D50}$.

In the discussion section, I compare the exponents m obtained here for the Swiss streams with steepness of the Φ_b vs. τ^* relation of Recking et al. (2016), i.e. Eq. (19). In general, it can be shown that the two dimensionless bedload transport variables W^* and Φ_b are related to each other as:

280 $$W^* = \Phi_b / \tau^{*1.5} \qquad (25)$$

For a given dimensionless reference shear stress, Eq. (19) can be simplified to:

$$\Phi_b = B\,\tau^{*(\alpha+\beta)} = \tau^{*p} \tag{26}$$

where B is a coefficient, $p = \alpha + \beta$, and the reference grain size for Φ_b may be D_{84} or D_{50}. Comparing Eq. (12), (25) and (26), the exponents can be related as follows:

285 $$m = \alpha + \beta - 1.5 = p - 1.5 \tag{27}$$

For the case of $\alpha = 2.5$ and $\beta = 4$ (Recking, 2012, 2013), this gives $m = \beta + 1 = 5$, and $p = m + 1.5 = \alpha + \beta + 1.5 = 6.5$.

2.4 Determining annual ratios of calculated to observed bedload masses based on observations for several years

If the analysis in section 2.3 can be related to medium time scales, involving durations of about 5000 to 20,000 minutes for each time window, the following analysis attempts to quantify the variability of annual bedload masses. The basis for this

290 analysis were extended datasets for the same four Swiss streams with typical observation durations of several years (Baldig and Rickenmann, 2024). The duration of active bedload transport for each year ranged from approximately 30,000 – 220,000 minutes and was therefore clearly longer than the time windows investigated in section 2.3. In this part, I essentially determined two ratios to quantify the year-to-year variability in a given stream and to compare these ratios between the four sites. The first ratio was defined as follows:

295 $$r_{x\_year} = MQ_{btot}/MQ_{bM} \tag{28a}$$

$$r_{x\_year} = MQ_{bred}/MQ_{bM} \tag{28b}$$

which represents the yearly calculated (MQ_{btot}, MQ_{bred}) divided by the observed (MQ_{bM}) bedload mass. In the index, x = "tot" or x = "red", according to the calculation with Q_{btot} or with Q_{bred}. The second ratio was defined as follows:

$$r_{x\_incQ} = slope\ of\ linear\ model\ between\ Cumsum(Q_{btot})\ and\ Cumsum(Q_{bM}) \tag{29a}$$

300 $$r_{x\_incQ} = slope\ of\ linear\ model\ between\ Cumsum(Q_{bred})\ and\ Cumsum(Q_{bM}) \tag{29b}$$

where the index "incQ" refers to the fact that here the yearly data was first ordered according to increasing Q values. Then a linear model was fitted to only those values for which $\tau^*_{D50} => 1.1\ \tau^*_{rD50}$ (for Eq. 29a) or for which $\tau^{*'}_{D50} => 1.1\ \tau^{*'}_{rD50}$ (for Eq. 29b). The reason for fitting the model only to values with larger flow intensities is motivated by the following arguments: (i) for larger flows, different bedload transport equations tend to predict more similar values (see e.g. Fig. 2), and (ii) the ratio

305 of the dimensionless bankfull shear stress to the dimensionless reference shear stress is approximately in the range 1.16 τ^*_{rD50} to 1.27 τ^*_{rD50}, and at bankfull flow considerable bedload transport may occur (Phillips and Jerolmack, 2019). Furthermore, I determined the ratio of calculated to observed bedload mass in chronological plots with cumulative sum values of Cumsum (Q_{bx})/Cumsum (Q_{bM}) as follows:

$$r_{x\_chron} = Cumsum(Q_{btot})\ and\ Cumsum(Q_{bM}) \tag{30a}$$

310 $$r_{x\_chron} = Cumsum(Q_{bred})\ and\ Cumsum(Q_{bM}) \tag{30b}$$

From these plots I determined a time duration for each year with begin of transport in spring, after which the ratio r_{x_chron} was approximately within a factor of three above or below the value r_{x_incQ}:

$$0.33\ r_{x\_incQ} < r_{x\_chron} < 3\ r_{x\_incQ} \tag{31}$$

12

Note that the ratios r_{t_year} and r_{r_year} (Eq. 28) are equivalent with the values r_{t_incQ} and r_{r_incQ} (Eq. 29), respectively, at the end

315 of a year.

3 Results

3.1 Comparison of observed bedload transport rates with predictive equations and mean annual trends for several years of observations

The bedload transport measurements at the five Swiss SPG-sites in Table 1 are compared in Fig. 3 to four different bedload
320 transport equations described in chapter 2 and in the Appendix A. The four bedload transport equations applied in Fig. 3 are
from Schneider et al. (2015a), namely SEA-1 (Q_{btot}, Eq. 5) and SEA-2 (Q_{bred}, Eq. 11), and the equation of Recking et al. (2016)
for β =4 (Eq. 14) using two different estimates of the reference shear stress, namely $\tau^*_{rRE\_min}$ (Eq. 17a, 18a, Q_{bRE_min}) and $\tau^*_{rRE\_ss}$
(Eq. 17b, 18b, Q_{bRE_ss}). Summary values characterizing the annual bedload transport for four streams and for the selected year
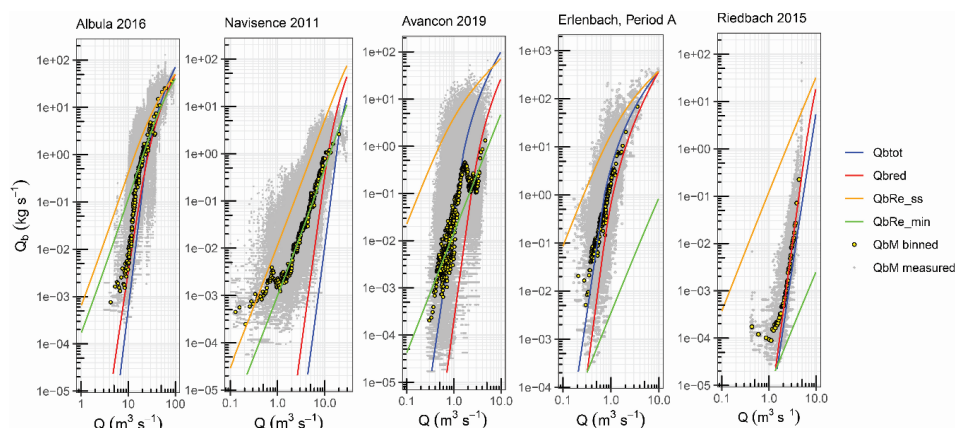are given in Table 4.

325

Figure 3. Comparison of bedload transport measurements (Q_b) at five Swiss streams with bedload transport calculations using for different predictive equations, shown as a function of discharge (Q). Erlenbach Period A refers to the years 1986 – 1999.

The first observation in Fig. 3 is a larger variability of measured Q_b values for a given discharge for the Navisence and the
Avançon sites than for the other three sites. For the sites of Albula, Erlenbach (Period A), and Riedbach, the Q_b vs. Q data are
more compact, and the mean trend, as determined by the geometric mean of the Q_b values for binned Q values, follows the
330 steepness defined by the two SEA equations quite closely (with m_{tot} =16.1 and m_{red} = 7.8). For the Navisence, the mean

observed trend follows the steepness defined by the Recking equation with β =4 (which is equivalent to m = 5.0, see Eq. 18) rather well. However, if further years or periods with SPG observations at the same sites are considered (similar plots for all available years are given in the Supplementary Material), the picture may change: For the Albula (Fig. S1, S2, S3), the mean trend for the steepness agrees better with the Recking equation with β =4 for the years 2017 and 2020; it generally agrees better

335   with the SEA equations for the year 2019; it has an intermediate steepness for the year 2018; and for the year 2021, the steepness is even lower than for the Recking equation with β =4. For the Navisence (Fig. S12, S13), the mean observed trend aligns better with the SEA equations for four years (2013, 2019, 2020, 2021); for the year 2012, however, the mean observed steepness is intermediate between the two types of equations. For the Avançon (Fig. S20, S21) the result is mixed. Three years align better with the SEA equations (2018, 2019, 2023) and three years align better with the Recking equation (2020, 2021,

340   2022). Finally, for the period B at the Erlenbach, the observed steepness is somewhat intermediate between the two types of equations (Fig. S28). In conclusion, the mean (annual) bedload rating curves are rather variable from year to year, and unsurprisingly, differ between sites.

3.2 Temporal variability of steepness of the bedload relation and of the reference shear stress for phase-2 transport conditions

345   The identified phase-2 transport conditions for the four Swiss streams analyzed in this part are given in Table 4. An illustration of the temporal variation of the bedload transport over the entire discharge range is shown in Fig. 4 (no such analysis was made for the Riedbach, due to the limited time resolution of the measured Q_b values and the relatively narrow Q_b vs. Q relation in Fig. 3). In Fig. 4, the distinction of mean trends for the Q_b vs. Q relations for phase-2 transport conditions between different double-weeks or sub-periods is rather clear for the Albula, the Navisence, and the Erlenbach (for both periods A and B).

350   However, the mean trends are less well defined for the Avançon. Generally, the trends in the steepness of these relations for the two-week periods are similar to the trends defined by geometric mean values over the entire year shown in Fig. 3.

The quantitative results regarding the determined values of the exponents m and the dimensionless reference shear stresses τ^*_{ref} are summarized in Table 5. The time-windows used to determine the trend lines (double weeks, sub-periods) involved durations of about 5000 to 20,000 minutes. The Supplementary Material provides a full list of all the individual values for each

355   stream (Table S1). In this quantitative analysis, not all time-windows (double week periods) shown in Fig. 4 yielded plausible results. This concerns the following number of excluded double week periods: 2 (out of 7) for the Albula, 1 (out of 10) for the Navisence, and 3 (out of 13) for the Avançon. All 13 sub-periods were used for the Erlenbach.
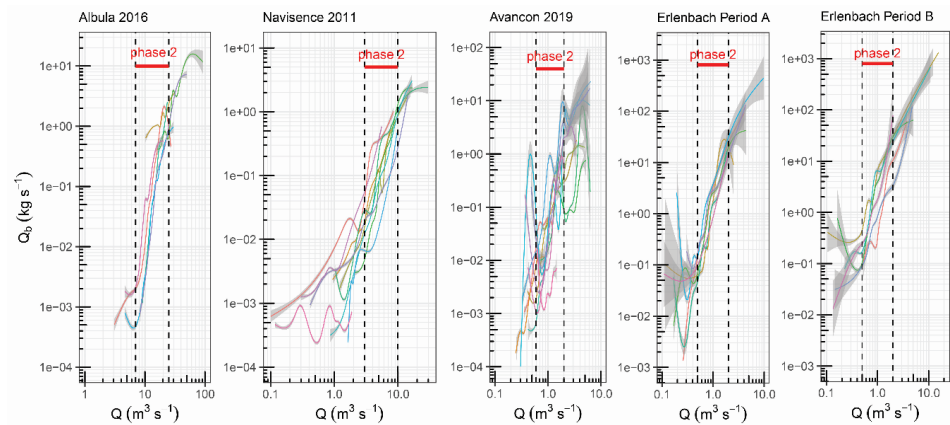
Figure 4. Temporal variability of bedload transport relations. The colored lines refer to the following time windows: for the Albula 7 consecutive double-week periods in summer 2016, for the Navisence 10 consecutive double-week periods in summer 2011, for the Avançon with 13 consecutive double-week periods in summer 2019, for the Erlenbach 7 sub-periods in period A (1986-1999) and 6 sub-periods in period B (2002-2016). The characteristic sub-periods for the Erlenbach were determined in Rickenmann (2024). The trend lines were determined by a loess smoothening function in the R code. The two black dashed lines and the red arrow denote the phase-2 transport conditions, which were used in the analysis described in section 2.3.

Table 5. Mean values of exponents m_{tot}, m_{red} and of dimensionless reference shear stresses τ^*_{rD50}, $\tau^{*'}_{rD50}$ derived from analysis of temporal variation of bedload transport relation for phase-2 transport conditions. A full list with all the individual values for each stream is given in the Supplementary Material (Table S1). For comparison, mean values of the variables from a similar analysis in Schneider et al. (2015a) for date sets "SEA_SS" and "SEA_HS" are also given here.

SPG site	year(s)	no. of time windows		W*tot analysis		W*red analysis	
				m_{tot}	τ^*_{rD50}	m_{red}	$\tau^{*'}_{rD50}$
Albula	2016	5 double-weeks	mean	13.63	0.040	9.15	0.026
Navisence	2011	9 double-weeks	mean	6.62	0.098	2.87	0.023
Avançon	2019	10 double-weeks	mean	11.94	0.121	4.57	0.020
Erlenbach A	1986-1999	7 sub-periods	mean	10.98	0.174	5.90	0.028
Erlenbach B	2002-2016	6 sub-periods	mean	10.75	0.172	5.79	0.028
SEA_SS	14 streams		mean	17.86	0.099	8.47	0.036
SEA_HS	21 streams		mean	7.51	0.037	5.15	0.028

360

15

A graphical illustration of the variability of m and τ^*_{ref} is presented in Fig. 5a for the W^*_{tot} analysis, and in Fig. 5b for the W^*_{red} analysis. Datasets from Schneider et al. (2015a), namely SEA_SS and SEA_HS, are also included in both figures. Note that a similar analysis as described in section 2.3 was performed in Schneider et al. (2015a) to determine values of m and τ^*_{ref} for

365   these latter data sets. Regarding the W^*_{tot} analysis, the mean m_{tot} values of the four Swiss streams generally fall between those of the SEA_SS and SEA_HS data sets (Table 5). The variability of the m_{tot} values for all the four Swiss streams (including temporal at-a-site and between-site variability) is in a similar range as for the SEA_SS and SEA_HS data sets (Fig. 5a). In general, the distribution of m and τ^*_{ref} for the Swiss streams is more similar to that for the SEA_SS data, whereas the SEA_HS data plot somewhat separately (Fig. 5a). ~~Interestingly, looking at~~ the τ^*rD50 values, ~~they~~ show a dependence for all the three
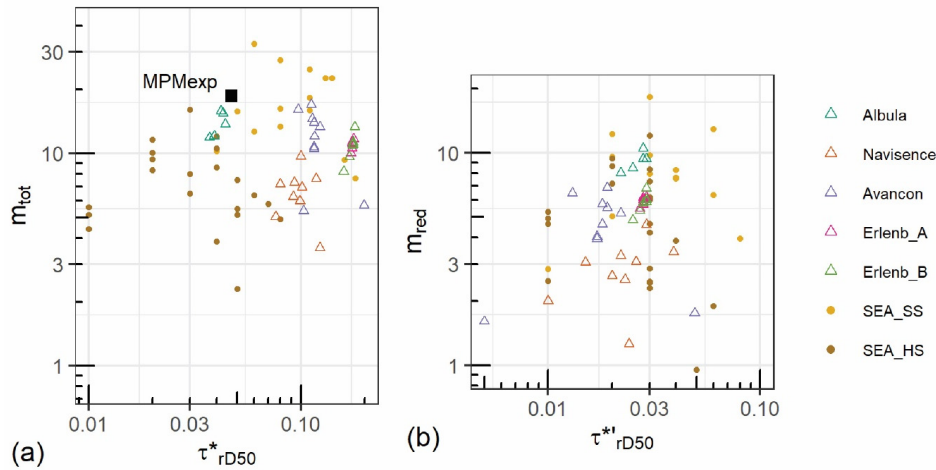
370   data sets on channel slope (Fig. 6).

Figure 5. Variability of (a) m_{tot} vs. the τ^*_{rD50} from W^*_{tot} analysis, and of (b) m_{red} vs. the $\tau^{*'}_{rD50}$ from W^*_{red} analysis. The legend is the same for both plots.

Turning to the W^*_{red} analysis, the mean m_{red} values of the four Swiss streams fall again between those of the SEA_SS and

375   SEA_HS data sets (Table 5). In general, the distribution of m and $\tau^{*'}_{ref}$ for the Swiss streams is more similar to that for the SEA_HS data, whereas the SEA_SS data plot somewhat separately (Fig. 5b). The mean $\tau^{*'}_{rD50}$ values for each of the four Swiss streams and for the SEA_SS and SEA_HS data sets range from 0.02 (Avançon) to 0.036 (SEA_SS) (Table 5). This is a typical range for Shield stresses or for τ^*_{ref} values for bedload transport equations based on a reduced or effective shear stress, with again a similar variability for each of the three data sets.
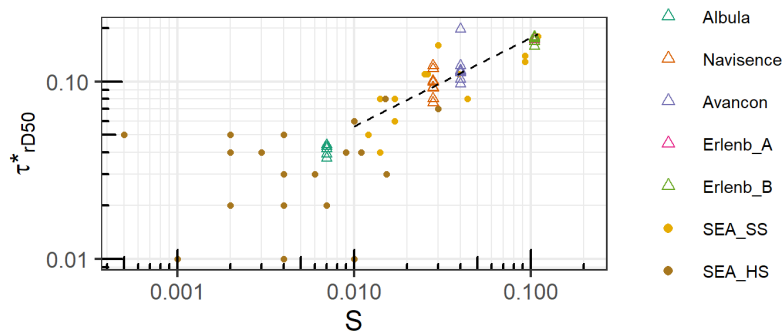
16

Figure 6. Variability of τ^*_{rD50} (from W^*_{tot} analysis) with channel slope. The dashed black line represents eq. (4), from a similar analysis in Schneider et al. (2015).

3.3 Variability of annual ratios of calculated to observed bedload masses determined for several years of observations

Annual ratios of calculated to observed bedload masses were determined based on observations over several years. For a given year this analysis was based on total durations with bedload transport, which ranged from about 30,000 to 150,000 minutes (only two years for the Navisence include longer durations). The main results of this analysis are summarized for all four Swiss streams in Table 6, while some additional information is given separately for each stream in the Supplementary Material (Tables S2, S3, S4, S5).

Table 6. Annual mean ratios of calculated to observed bedload masses, and results of cumulative sum analysis. See text and list of symbols for meaning of variables. A full list with all the individual values for each stream is given in the Supplementary Material (Tables S2, S3, S4, S5).

SPG site	Year	Minutes	r_{t_year}	r_{t_incQ}	r_t within factor 3 from X minutes	r_{r_year}	r_{r_incQ}	r_r within factor 3 from X minutes
Albula	2016	78761	0.570	0.614	33000	0.442	0.453	25000
Albula	2017	24668	0.108	0.294	16000	0.132	0.255	9000
Albula	2018	36888	0.253	0.251	3200	0.224	0.210	2100
Albula	2019	44633	0.907	0.796	5700	0.670	0.597	5600
Albula	2020	39952	0.230	0.336	29000	0.185	0.264	29000
Albula	2021	27076	0.162	0.218	19000	0.134	0.177	18000
Albula	2022	22171	0.035	0.260	NA	0.067	0.243	NA
Albula	2023	43890	0.584	0.910	37000	0.428	0.663	37000
	mean	*39755*	*0.356*	*0.460*	*20414*	*0.285*	*0.358*	*17957*
Navisence	2011	186439	0.066	1.575	NA	0.437	5.724	NA

17

Navisence	2012	220319	0.049	0.590	NA	0.630	2.949	NA
Navisence	2013	142384	0.461	0.704	(73000)	2.991	2.653	73000
Navisence	2019	66436	0.490	1.423	32000	3.055	5.430	25000
Navisence	2020	117214	0.384	1.914	NA	3.002	8.468	57000
Navisence	2021	105612	0.879	3.067	(24000)	7.043	14.500	19000
	mean	*139734*	*0.388*	*1.546*		*2.860*	*6.621*	*43500*
Avancon	2018	139106	5.663	8.135	28000	0.882	0.973	30000
Avancon	2019	146560	5.221	6.287	23000	1.460	1.459	25000
Avancon	2020	90302	3.593	6.588	16000	0.386	0.577	20000
Avancon	2021	23608	5.875	7.389	4700	0.588	0.700	5000
Avancon	2022	37562	4.633	4.793	6700	1.954	1.519	16000
Avancon	2023	95707	11.346	14.420	91	2.820	2.436	216
	mean	*88808*	*6.055*	*7.935*	*13082*	*1.349*	*1.277*	*16036*
Erlenbach	Period-A	37930	0.840	0.994	0	0.248	0.163	3100
Erlenbach	Period-B	33917	0.817	0.940	3800	0.343	0.218	4700
	mean	*35924*	*0.829*	*0.967*	*1900*	*0.295*	*0.191*	*3900*

A graphical example for the determination of the ratios r_{t_incQ} and r_{r_incQ} with a linear model fitted to the function Cumsum

390   (Q_{bx}) vs. Cumsum (Q_{bM}), x = tot or red, for the flow intensities $\tau^*_{D50} => 1.1\ \tau^*_{rD50}$, is given for the Albula in 2019 in Fig. 7a.

The values of r_{t_incQ} and r_{r_incQ} were then compared with the chronologically determined ratios Cumsum (Q_{bx}) to Cumsum (Q_{bm}), i.e. the r_{t_chron} and r_{r_chron} values, for each year. Fig. 7b illustrates this for the Albula in 2019. This allowed to derive the approximate duration from the beginning of the transport season to the time point after which the r_{x_chron} values were within about a factor of 3 above or below the r_{x_incQ} values, x = t or r. These limiting deviations are illustrated by dashed and dotted

395   lines in Fig. 7b, indicating that the relative agreement of calculated to observed bedload masses only varied in a limited range after this time point. In the Supplementary Material similar diagrams are given for all years of the Albula (Fig. S4 to S11), the Navisence (Fig. S14 to S19), the Avançon (Fig. S22 to S27), and the Erlenbach (Fig. S29 to S30).

A similar picture becomes apparent when comparing the ratios r_{t_year} and r_{r_year} (Fig. 8a) and the ratios r_{t_incQ} and r_{r_incQ} (Fig. 8b) for the four streams, for both the W^*_{tot} analysis and for the W^*_{red} analyses: While there is a tendency to under-estimate the

400   observed bedload masses for two streams (Albula, Erlenbach), a tendency for an over-estimation is apparent for the other two streams (Navisence, Avançon). The variability of the ratios for a given stream and type of analysis (W^*_{tot} or W^*_{red}) is similar for all cases. The effect of flow or transport intensity on the ratios r_{t_year} (Fig. 9a) and r_{r_year} (Fig. 9b) was considered by plotting these ratios against $Q_{max}/Q_{1.1}$, where Q_{max} is the maximum water discharge for a given year and $Q_{1.1}$ is the water discharge corresponding to a dimensionless shear stress $\tau^*_{D50} = 1.1\ \tau^*_{rD50}$ (Table 3). For the Albula, the ratios indicate that the calculated

405   and observed bedload masses are more closely aligned at higher flow intensities. For the other three streams, no clear trend

18

appears. However, when accounting for all the stream sites, one may see a slight trend towards increased agreement between the calculated and observed bedload masses for increasing flow intensities This is somewhat clearer for the W^*_{red} analysis than for the W^*_{tot} analysis.
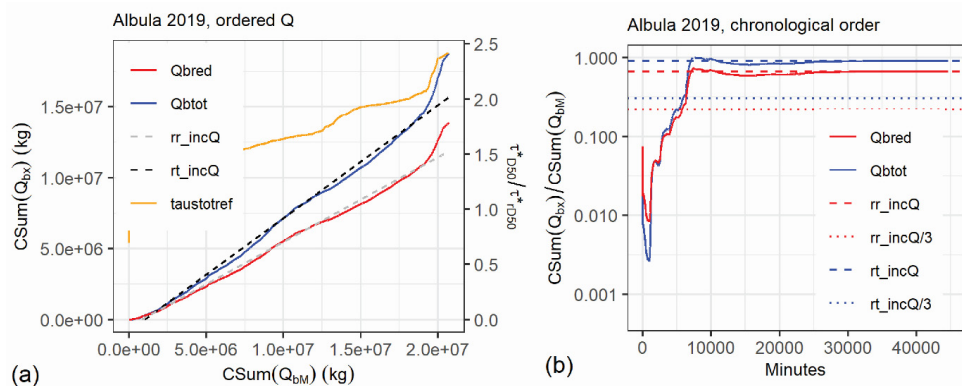

Figure 7. Albula, summer 2019. Example of a good agreement of a liner model (dashed black and gray lines) for the cumulative sum of calculated ($CSum(Q_{bx})$) vs. measured ($CSum(Q_{bM})$) bedload masses. In (a) the values were ordered according to increasing discharge Q, and the increase in relative flow intensity is shown with the ratio $\tau^*_{D50}/\tau^*_{rD50}$ (taustotref). In (b) the values are summed up in chronological order.

410
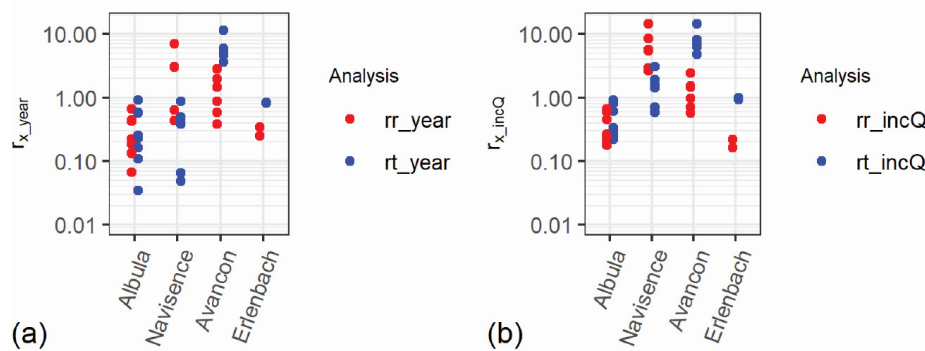
Figure 8. Variability of (a) r_{x_year} and (b) r_{x_incQ}, separately for the analysis with the Q_{btot} calculations (x=t) and for the Q_{bred} calculations (x=r)
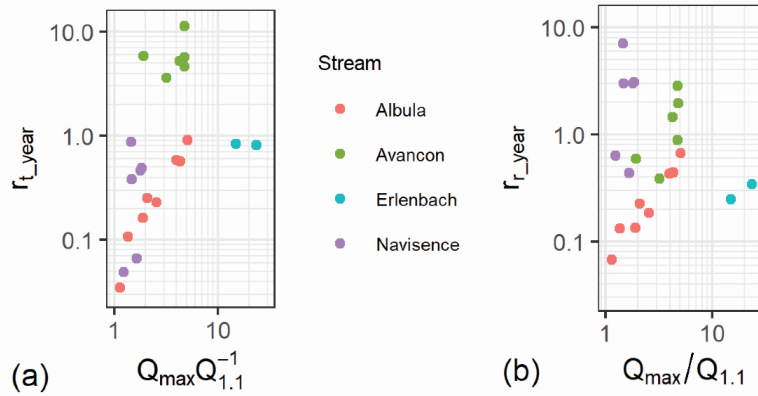
19

Figure 9. Variability of (a) r_{t_year} and (b) r_{r_year}, plotted against normalized maximum discharge ($Q_{max}/Q_{1.1}$) in each year.

For a given stream with several years of observations, the 15 mean values of the four ratios r_{t_year}, r_{r_year}, r_{t_incQ}, and r_{r_incQ} typically vary in a range of about 0.3 to 3, with two smaller r values (r_{r_year} for the Albula, r_{r_incQ} for the Erlenbach) and with

415   two larger r values (r_{t_year} for the Avançon, r_{r_incQ} for the Navisence) (Table 6). Thus, considering a time-period of several years, the mean annual ratios of predicted to measured bedload masses are roughly within a factor of 3 above and below a perfect agreement.

4 Discussion

4.1 General comments on the steepness of the bedload transport equations

420   The MPM equation has often been applied in studies on gravel-bed rivers, and it is implemented in many numerical software codes to simulate bedload transport, typically for longer river reaches in 1D or also in also in selected river reaches in 2D simulations. Such software tools include HEC-RAS (Yavuz, 2025), Telemac (Villaret et al., 2013) and Basement (Bürgler et al., 2020). As can be seen in Fig. 2, the original MPM equation has an important drawback, in that the predicted transport rates in the vicinity of the Shields number τ^*_c almost encounter a step-function because the MPM relation (Eq. 20, hereafter referred

425   to as original MPM) approaches a vertical line for dimensionless shear stresses slightly larger than but approaching the τ^*_c value. Therefore, it is much more sensitive in this shear stress range to the choice of the characteristic grain size D_{50}, which is typically needed to estimate an appropriate τ^*_c or τ^*_{ref} value, than the other equations. Four of the other predictive equations in Fig. 2 use a dimensionless reference shear stress, and the exponential form of the MPM equation (Eq. 22, hereafter referred to as MPMexp) results in a bedload transport relation that is qualitatively more similar to the SEA and the Recking equations

than to the original MPM equation. For comparison, the mean steepness of Eq. (22) in Fig. 2c was calculated for bedload transport intensities in the range $1e-7 < W^* < 0.002$ (the larger value corresponding to a dimensionless reference hear stress = 0.047) by approximating a power law, and this gives an equivalent exponent of $m = 18.7$. This value is rather close to the characteristic values for the SEA_SS data set, with a mean $m = 17.9$ (Table S1) and a median $m = 16.1$ which is used in Eq. (2a) to calculate W^*_{tot} or Q_{btot}. The value of $m = 18.7$ for $\tau^*_{ref} = 0.047$ for the MPMexp equation in the given range of W^* values is included in Fig. 5 for comparison; this data point is positioned at the outer perimeter of the CH_TV and the SEA_SS data.

If the Recking equations (19, 18a, 18b) are presented in the W^* vs. τ^*_{D50} (or τ^*_{D84}) form, the exponent (steepness) is $m = 5$ (Fig. 2, Eq. 27). Thus, they define flatter bedload transport relations for small to medium flow intensities than the SEA equations (2) and (9), and for the three Swiss streams with channel slopes smaller than 5% (Albula, Navisence, and Avançon) they tend to predict larger transport rates than the latter (Fig. 2, 3). In the Φ_b vs. τ^*_{D50} (or τ^*_{D84}) representation, the exponent p for the steep part is (Eq. 26) $p = 6.5$ for the Recking equation (19), and $p = 17.6$ for the SEA-1 equation (2a) and $p = 9.3$ for the SEA-2 equation (9a). Thus, the steepness of the SEA-equations is considerably larger than those of Eq. (14, 19, 26) with $\alpha = 2.5$ and $\beta = 4$. The range of steepness values for the two types of equations, when adapted to measured bedload transport rates, is discussed in the following discussion section.

4.2 Comparison of the steepness and the dimensionless reference shear stress with the REA study

In this section I compare the range of values obtained by analyzing the temporal variation of the bedload relations for phase-2 transport in the four Swiss streams (section 3.2) with the results reported in Recking et al. (2016; "REA study"). Henceforth the data set of the four Swiss streams for the analysis of m and τ^*_{ref} (as included in Fig. 5 and 6; section 3.2) is labeled "CH_TV" (TV for temporal variation), and the data set of Recking et al. (2016) is labeled "REA_BT" (BT for β and τ^*_{ref}) henceforth; these labels are used in Fig. 10, 11, and 12 below.

As a caveat it must be mentioned that Recking et [...] 016) varied either the exponent β (steepness) of Eq. (14, 19) or the reference shear stress τ^*_{refRe}, to find a good agreement of the predictions with the measurements, while the other variable was prescribed. Namely (case 1 analysis) they fixed $\beta = 4$ when optimizing the τ^*_{refRe} values, or (case 2 analysis) when optimizing the β values they set τ^*_{refRe} as a function of the channel slope as:

$$\tau^*_{refRe} = 0.26\ S^{0.3} \tag{32}$$

which is based on flume experiments and should provide a better link of Eq. (14) with the bedload transport measurements in flume experiments. For the results obtained in this study for the four Swiss streams in section 3.2, however, both the exponents m and the τ^*_{ref} values were optimized in the same step (section 2.3). For their case 1 analysis, Recking et al. (2016) found a strong dependence of the τ^*_{refRe} values for plane beds on channel slope, approximated with a power law relation as:

$$\tau^*_{refRe} = 1.5\ S^{0.75} \tag{33}$$

My results for the τ^*_{rD50} values based on the W^*_{tot} analysis in Fig. 6 compare fairly well with the results of Recking et al. (2016) as illustrated in Fig. 10. The power law relation (33) is quite similar to a relation found by Schneider et al. (2015a) for the SEA_HS data set using total shear stress (for which both the exponents m and the τ^*_{ref} values were optimized). On the other hand, the relation obtained by Schneider et al. (2015a) for the SEA_SS data set using total shear stress (Eq. 2a) lies

465   between the two power law relations (32) and (33). However, for channel slopes in the range $0.01 < S < 0.1$, the τ^*_{ref} values predicted by (32) and (33) are similar to those predicted by Eq. (4), as can also be seen by comparing Fig. 6 and 10. These results suggest that a comparison between the two approaches may be justified.
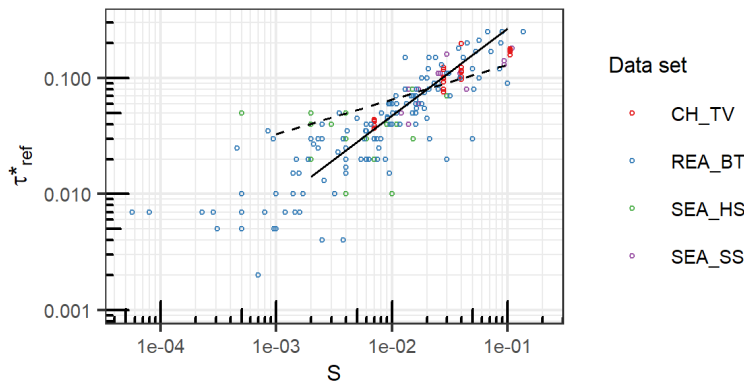

Figure 10. Optimized values of τ^*_{ref} vs. channel slope S, for various datasets. For the CH-TV, SEA_SS and SEA_HS data, τ^*ref f was determined based on a W^*_{tot} analysis. For the REA_BT data, τ^*_{ref} was derived from the Recking equation assuming a fixed exponent $\beta = 4$ (case 1 analysis). The solid black line is eq. (24) derived from the REA_BT data with a plane-bed morphology. The dashed black line is eq. (23) from Recking et al. (2016) based on flume experiments and used in their case-2 analysis.

470   Turning now to the case 2 analysis of Recking et al. (2016), the range of their optimized β values depends to some extent on channel slope (Fig. 11a). This is in contradiction to the ranges of the β values from the CH_TV and the SEA_SS data set together (converted from m values with Eq. 27) (Fig. 12), for which only the β values for the largest slope class (0.02,0.2] from the W^*_{red} analysis approximately agree with the β values of Recking et al. (2016) for the same slope class. If we consider only the SEA_HS data, the β values from the W^*_{red} analysis (Fig. 11b) agree better with the β values of Recking et al. (2016) for

475   the same slope class (Fig. 11a) than the β values from the W^*_{tot} analysis (Fig. 11c).
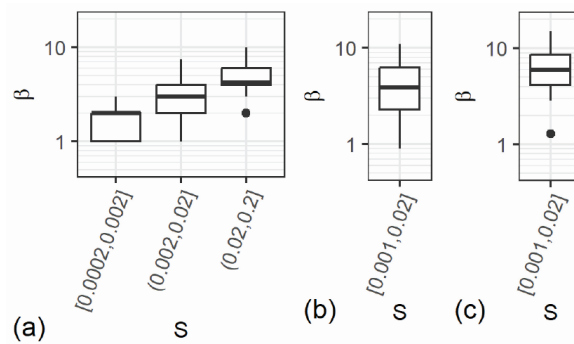
22

Figure 11. Boxplots of the exponent β for different for channel slope classes. (a) for the entire REA_BT data, for the case 2 analysis assuming eq. (23) to pre-define the τ^*_{ref} values, (b) for the SEA_HS data, derived from the W^*_{red} analysis, (c) for the SEA_HS data, derived from the W^*_{tot} t analysis. For the SEA_HS data from Schneider et al. (2015), 19 out of 21 data points fall into the slope class shown here.
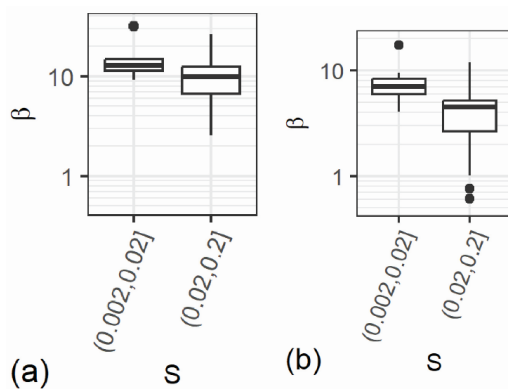

Figure 12. Boxplots of β for the CH_TV and SEA_SS data combined, for 2 slope classes, derived (a) from the W^*_{tot} analysis, and (b) from the W^*_{red} analysis.

4.3 Possible implications of the above comparison and some limitations

480   In summary, the results of the case 1 analysis of Recking et al. (2016) regarding the τ^*_{ref} values are roughly in better agreement with the W^*_{tot} analysis of the Swiss streams and the SEA_SS data. Conversely, the results of their case 2 analysis regarding the β or m values are roughly in better agreement with the W^*_{red} analysis of the Swiss streams and the SEA_HS data. This

suggests that the bedload transport equation of Recking et al. (2016), using D_{84} for the definition of Φ_{b84} and of τ^*_{D84}, is an approach somewhere intermediate between the bedload transport equations SEA-1 (W^*_{tot}) and SEA-2 (W^*_{red}), using D_{50} as a

485 reference grain size. It is likely that the use of a slope-dependent τ^*_{ref} value (Eq. 23) in the case 2 analysis resulted in a channel slope-dependence of the optimized β values (Fig. 12a): Eq. (32, case 2) and Eq. (33, case 1) cross each other at about $S = 0.02$. For $S > 0.2$, τ^*_{ref} (Eq. 32) is smaller than τ^*_{ref} (Eq. 33) (Fig. 10) which has to be compensated by a value β > 4 (Fig. 11a) to result in a similar bedload transport level for the two analyzed cases; conversely, for $S < 0.2$, τ^*_{ref} (Eq. 32) is larger than τ^*_{ref} (Eq.33) (Fig. 10) which has to be compensated by a value β < 4 (Fig. 11a).

490 Recking et al. (2016, and their Fig. 9) argued that their approach (Eq. 14) using D_{84} as a reference grain size is roughly equivalent to using a reduced or effective shear stress with D_{50} as a reference grain size, by showing that for their data set τ^*_{D84} $\ll \tau^*_{D50}$ and $\tau^*_{D84} \approx \tau^{*\prime}_{D50}$, where the latter values were determined with a similar approach as used for the SEA equations. For our data sets with the four Swiss streams, a similar comparison was made (Fig. S31), confirming a similar pattern for three sites (except for the Albula site, for which $\tau^*_{D84} \ll \tau^{*\prime}_{D50}$ was observed). The analysis above showed, however, that the results

495 of Eq. (14) are not directly comparable with the results of the W^*_{red} equation (9). Two other elements may also contribute to the fact that the approach of Eq. (14) generally requires smaller β or m values than Eq. (9), particularly for channel slopes smaller than about 0.02. First there is the problem that the Helley-Smith sampler applied in gravel bed streams tends to over-sample at low and to under-sample at higher transport intensities, resulting in a generally less steep bedload vs. discharge relation (Bunte and Abt, 2005; Bunte et al., 2008; Schneider et al., 2015a). The β values of the W^*_{red} analysis (Eq. 9) for the

500 SEA_HS data are about in the range of 2 to 6 (Fig. 11b), and the β values of REA_BT data in the range of 2 to 4 for the same slope class (Fig. 11a); this slight difference may be associated with somewhat smaller $\tau^{*\prime}_{D50}$ values found for the SEA_HS data (Schneider et al., 2015a, Fig. 3b therein) than those pre-defined for the case 2 analysis using Eq. (32). Second, an inspection of the REA_BT dataset showed that for about half these streams a temporal variation of the measured bedload transport data could be identified (for 47 streams I could identify reliable time and date data, and the Q_b vs. Q data showed a

505 time-dependence for 23 streams, no time-dependence for 18 streams, and the patterns was inconclusive for 6 streams); if such bedload transport data is averaged arithmetically it may lead to lower β or m values, because this neglects a lateral shift of the transport relation as observed for the four Swiss streams (Fig. 4).

The analysis of the beta exponents of Recking et al. (2016) showed that the steepness of the bedload relation is generally somewhat steeper and more variable in mountain streams, i.e. for plane bed and step-pool streams as compared to streams with

510 a riffle-pool or braided morphology, than for wider streams with a flatter channel slope. A possible reason for this may be that more fine particles are available in flatter streams, leading to larger transport and generally lower β or m values according to the Recking Eq. (14). Recking et al. (2016) also found that for riffle-pool morphologies the grain-size distribution, likely a proxy for the riffle-pool development, influences the optimal reference shear stress. In general, both the Recking equation (14) and the two SEA equations (2) and (9) are considered to provide a useful reference calculation framework for bedload transport

515 levels, which can be used to quantify other influencing factors (apart from the hydraulic forcing), such as sediment supply or

availability and bed morphology, that can help to further constrain the variables steepness (exponent) and reference shear stress in these approaches. However, to better quantify such effects both continuous bedload transport measurements are needed along with more detailed information on streambed characteristics and sediment availability.

4.4 Annual ratios of calculated to observed bedload masses

520 In general, many bedload transport equations have an exponent $p = 1.5$ in a Φ_b vs. τ^* relation (Eq. 26) for large flow and transport intensities (including Eq. 2, 9, 20, 22), and this implies that the bedload transport rate Q_b is approximately linearly related to discharge Q (see also Fig. 2a). This motivated the analysis outlined in section 2.4 with the results presented in section 3.3. Although there is still considerable variability of the annual ratios shown in Fig. 8 and 9, the four ratios r_{t_year}, r_{r_year}, r_{t_incQ}, and r_{r_incQ} typically vary in a range of about 0.33 to 3 for a given stream (Table 6), thus confirming the motivation for this

525 analysis.

Evidence for such an approximately linear relation between yearly observed bedload masses and simple measures of flow intensity were already presented for the Erlenbach (Rickenmann, 1997; Rickenmann, 2020, Fig. S7 therein), and for the Albula and the two Austrian mountain streams Fischbach and Ruetz (Rickenmann, 2018; Rickenmann et al., 2020). In Rickenmann (2018, Fig. S15 therein) it was shown that the ratio sum (Q_{bM}) / sum (Q) converged to an agreement within a factor of 2 after

530 about 50 to 60 days of transport for both Austrian streams. For the Erlenbach and the other two streams, the yearly sum (Q_{bM}) values also showed a correlation with the yearly excess runoff volume V_{re} = sum (Q- Q_c), multiplied by (the normalized) maximum discharge (Rickenmann, 1997; Rickenmann et al., 2020). Q_c is a critical discharge above which more intense bedload transport starts. For the four Swiss streams of this study a similar analysis confirmed this earlier empirical finding of an approximately linear relation between either yearly observed bedload masses calculated with Eq. (9) or yearly measured

535 bedload masses and a simple measure of the yearly flow intensity (Fig. 13). In this context it is of interest, that the analysis of several bedload-transporting flood events in Summer 2005 in Switzerland also confirmed the existence of such an approximately linear relation between observed bedload masses and simple measures of flow intensity, integrated over the flood event duration (Rickenmann and Koschni, 2010). Further independent evidence of a better agreement between calculated and measured bedload transport levels for higher or longer flow intensities is presented by Recking et al. (2012), who found a

540 clearly increasing agreement between calculated and observed transport for either longer integration periods and/or relative flow intensities τ^*/τ^*_c larger than about 1.2.
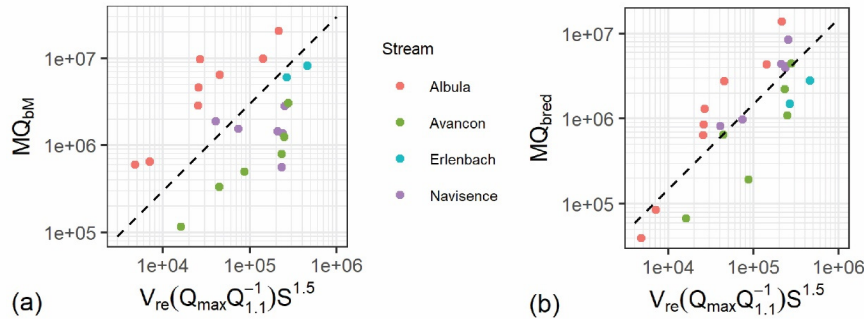
Figure 13. Yearly bedload masses vs. a simple measure of flow strength, as V_{re} (Q_{max}/Q_1.1) $S^{1.5}$. (a) for the measured yearly bedload mass, sum (Q_{bM}), and (b) for the calculated yearly bedload mass using eq. (9), sum (Q_{bred}). The dashed black lines indicate a linear relation, the position of which was chosen to approximately fit the trend defined by the data of the four streams.

5 Conclusions

This study examined how bedload transport may vary in time and space. The analysis was based on continuous and long-term

545   bedload transport surrogate measurements in several Swiss mountain streams using the Swiss Plate Geophone monitoring system. This indirect measuring system had been calibrated in previous studies to produce reliable estimates of bedload transport rates. The main findings and conclusions of the study are summarized as follows.

1. Bedload transport changes significantly during shorter time intervals such as a few weeks in larger streams or over a number of sediment-transporting flow events in a small mountain torrent. This variability was quantified in terms of the steepness and

550   the reference shear stress of the two types of bedload transport equations proposed by Schneider et al. (2015a): one based on total bed shear stress and the other on a reduced bed shear stress formulation.

2. When bedload transport was aggregated yearly, i.e. over longer time scales, predictions from the above-mentioned equations agreed with measured values roughly within a factor of three, although some streams consistently showed over- or under-estimates. A potentially important finding for engineering applications is that yearly aggregated bedload masses depended

555   approximately linearly on a simple measure of flow intensity, namely the integrated excess discharge.

3. The variability of the steepness and the reference shear stress is roughly in a similar range to that observed in a comprehensive study by Recking et al. (2016), which included direct bedload transport measurements from more than 100 streams; however, this only applies when channel slopes larger than about 2 % are considered. For the streams with channel slopes smaller than about 2 %, the Recking-study determined steepness values that are generally smaller than those found for

560   the four Swiss streams and a data set in Schneider et al. (2015a), possibly due to a higher availability of fine particles in flatter streams.

4. The original form of the Meyer-Peter and Müller bedload transport equation is not suitable for bedload calculations over the entire discharge range and in particular for small and intermediate flow intensities in the vicinity of the critical dimensionless shear stress, because there is a step-like discontinuity in this range. An exponential form of the Meyer-Peter and Müller equation is more similar to the reference shear-stress based formulations (used in this study) and performs better in this range. However, a characteristic steepness of this equation is at the edge of the values resulting from the application of the bedload transport equation of Schneider et al. (2015a) based on total bed shear stress.

Data availability

The data sets for the Riedbach (Schneider et al., 2016), the Erlenbach (Rickenmann, 2020, 2024), and the Avançon (Antoniazza et al., 2022) were already published and are available online in the EnviDat repository: https://www.envidat.ch/#/metadata/sediment-transport-observations-in-swiss-mountain-streams (Rickenmann et al., 2023). The bedload transport data for the Albula 2016 and for the Navisence 2011 will be available online in the EnviDat repository as well (upon final publication).

Supplement

The supplement related to this article is available online at: xxxx.

Appendix A. Flow resistance calculations

All flow resistance calculations are based on discharge-based equations using the following dimensionless variables for velocity U^{**} and for unit discharge q^{**} (Rickenmann and Recking, 2011):

$$U^{**} = U/\sqrt{gSD_{84}} \tag{A1a}$$

$$q^{**} = q/\sqrt{gSD_{84}^3} \tag{A1b}$$

where U = mean flow velocity, S = channel slope D_{84} = characteristic grain size of the bed surface for which 84% of the particles are finer, q = unit discharge, and g gravitational acceleration.

For the Erlenbach, the hydraulic calculations were carried out with an equation given in Nitsche et al. (2012, Fig. 5d therein),

590   based on dye tracer measurements made in the lowermost reach:

$$U^{**} = 1.49\, q^{**^{0.6}} \tag{A2}$$

For the Riedbach, the hydraulic calculations were carried out with an equation given in Schneider et al. (2016), also based on dye tracer measurements made in the lowermost reach:

$$U^{**} = 1.74\, q^{**^{0.6}} \tag{A3}$$

595   For the other three sites Albula, Navisence, and Avançon, the following equation of Rickenmann and Recking (2011) was used:

$$U^{**} = 1.443\, q^{**^{0.6}} (1 + (q^{**}/43.78)^{0.8214})^{-0.2435} \tag{A4}$$

The unit discharge q was determined for a mean width for a given flow depth in the trapezoidal cross-section, and bank resistance was accounted for by reducing q with the ratio of the hydraulic radius r_h to the flow depth h. This required an

600   iterative calculation procedure, using the measured discharge Q along with the trapezoidal cross-section.

Appendix B. List of variables

A_c	size of catchment area (km^2) at the location of the SPG measuring site
D_{xx}	grain size of the bed surface for which xx% of the particles are finer
IMP	impulse counts per minute (using the SPG system)
k_{isp}	calibration coefficients determined for each survey interval at the Erlenbach
k_{site}	calibration coefficients determined for the Albula, Navisence, and Avançon
m	Exponent in Eq. (2), general term including m_{tot} from W*$_{tot}$ analysis and m_{red} from W*$_{red}$ analysis
MQ_{bM}	sum of Q_{bM} per year, multiplied with 60 s, to give the yearly transported bedload mass
MQ_{bred}	sum of Q_{bred} per year, multiplied with 60 s, to give the yearly calculated bedload mass
MQ_{btot}	sum of Q_{btot} per year, multiplied with 60 s, to give the yearly calculated bedload mass
Q	water discharge (m^3 s^{-1})
Q_{max}	maximum water discharge (m^3 s^{-1}) in a given year
$Q_{1.1}$	water discharge (m^3 s^{-1}) corresponding to a dimensionless shear stress $\tau*_{D50} = 1.1\ \tau*_{rD50}$ (Table 3)
q_b	volumetric bedload transport rate per unit width (m^3 s^{-1})
Q_{bm}	measured bedload transport rate (Eq. 1) (kg s^{-1})
Q_{bM}	measured bedload transport rate, zero values replaced by mean with neighboring non-zero values (kg s^{-1})
Q_{bred}	calculated bedload transport rate, based on the reduced (effective) shear stress (Eq. 9)
Q_{btot}	calculated bedload transport rate, based on the total shear stress (Eq. 2)
Q_{bz}	measured bedload transport rate, including zero values
Q_{max}	peak discharge of an event
$r_{t\ chron}$	ratio of Cumsum (Q_{btot}) / Cumsum (Q_{bm}) [Eq. 30a]
$r_{r\ chron}$	ratio of Cumsum (Q_{bred}) / Cumsum (Q_{bm}) [Eq. 30b]

$r_{t\ incQ}$	slope of linear model between Cumsum (Q_{btot}) and Cumsum (Q_{bm}) [Eq. 29b]
$r_{r\ incQ}$	slope of linear model between Cumsum (Q_{bred}) and Cumsum (Q_{bm}) [Eq. 29b]
$r_{t\ year}$	ratio of MQ_{btot}/MQ_{bM} [Eq. 28a]
$r_{r\ year}$	ratio of MQ_{bred}/MQ_{bM} [Eq. 28b]
$R2$	squared Pearson correlation coefficient
$s = \rho_s/\rho$	relative sediment density, with ρ_s = sediment density and ρ = water density
S	channel slope of natural channel-reach upstream of SPG site
S'	reduced energy slope (associated with a reduced or effective shear stress)
u^*	the shear velocity (m s^{-1})
U	mean flow velocity (Appendix A)
w	channel width
W^*	dimensionless bedload transport rate, $W^* = (s-1)\ g\ q_b\ /\ u^{*3}$ [Eq. 13]
Φ_b	dimensionless bedload transport rate, $\Phi_b = q_b\ /\ \mathrm{sqrt}((s-1)\ g\ D^3)$ [Eq. 15, 21]
τ^*	dimensionless total bed shear stress = $(g\rho r_h S)\ /\ (g\rho(s-1)D_{xx})/$
τ'	dimensionless reduced or effective bed shear stress $(g\rho r_h S')\ /\ (g\rho(s-1)D_{xx})$
τ^*_c	dimensionless critical shear stress (at beginning of motion)
τ^*_{D50}	dimensionless total bed shear stress (for W^*_{tot}, Eq. 2), with reference to D_{50}
$\tau^{*'}_{D50}$	dimensionless reduced bed shear stress (for W^*_{red}, Eq. 9), with reference to D_{50}
τ^*_{Re84}	dimensionless total bed shear stress (for Φ_{b84}, Eq. 14, 19), with reference to D_{84}
τ^*_{ref}	dimensionless reference shear stress, general term including τ^*_{rD50} from W^*_{tot} analysis, $\tau^{*'}_{rD50}$ from W^*_{red} analysis, and τ^*_{refRe} in Eq. (19)

References

Aigner, J., Kreisler, A., Rindler, R., Hauer, C. & Habersack, H. (2017) Bedload pulses in a hydropower affected alpine gravel bed river. Geomorphology, 291, 116–127. Available from: https://doi.org/10.1016/j.geomorph.2016.05.015

605 Ancey, C. (2020) Bedload transport: a walk between randomness and determinism. Part 1. The state of the art, J. Hydraul. Res., 58, 1–17, https://doi.org/10.1080/00221686.2019.1702594

Antoniazza, G., Nicollier, T., Boss, S., Mettra, F., Badoux, A., Schaefli, B., Badoux, A., Rickenmann, D. & Lane, S.N. (2022) Hydrological drivers of bedload transport in an Alpine watershed. Water Resour. Res., 58(3), e2021WR030663, https://doi.org/10.1029/2021WR030663

610 Antoniazza, G., Dietze, M., Mancini, D., Turowski, J. M., Rickenmann, D., Nicollier, T., Boss, S. & Lane, S.N. (2023) Anatomy of an Alpine bedload transport event: A watershed-scale seismic-network perspective. J. Geophys. Res.-Earth, 128, e2022JF007000, https://doi.org/10.1029/2022JF007000

Baldig & Rickenmann (2024) Schweizer Plattengeophon (SPG): Umrechnung von Paketdaten in fraktionierte Geschiebetransportraten und einige Analysen dazu. Eidgenössische Forschungsanstalt für Wald, Schnee und Landschaft,
615 internal report, 31. Oktober 2024.

Bagnold, R.A. (1966) An approach to the sediment transport problem from general physics. U.S. Geological Survey Professional Paper 422-I.

Buffington, J.M., & Montgomery, D.R. (1997) A systematic analysis of eight decades of incipient motion studies, with special reference to gravel-bedded rivers. Water Resour. Res., 33(8), 1993–2029. https://doi.org/10.1029/96WR03190

620   Bunte, K. & Abt, S.R. (2005) Effect of sampling time on measured gravel bed load transport rates in a coarse-bedded stream. Water Resour. Res., 41, W11405, doi:10.1029/2004WR003880.

Bunte, K., Abt, S.R., Potyondy, J.P. & Swingle, K.W. (2008) A comparison of coarse bedload transport measured with bedload traps and Helley-Smith samplers. Geodin. Acta, 21(1–2), 53–66, doi:10.3166/ga.21.53-66.

Bürgler, M., Vetsch, D.F., Boes, R.M., Vanzo, D. (2022). Systematic comparison of 1D and 2D hydrodynamic models for the
625   assessment of hydropeaking alterations. River Res. Appl., 39(3), 460–477, https://doi.org/10.1002/rra.4051

Cheng, N.-S. (2002) Exponential formula for bedload transport. J. Hydraul. Eng., 128(10), 942–946, https://doi.org/10.1061/(ASCE)0733-9429(2002)128:10(942)

Church, M. (2006) Bed material transport and the morphology of alluvial river channels. Annual Review of Earth and Planetary Sciences, 34(1), 325–354.

630   Church, M. (2010) Chapter 2: Mountains and montane channels. In T. Burt & R. Allison (Eds.), Sediment cascades (pp. 17–53). Oxford, UK: John Wiley-Blackwell.

Coviello, V., Vignoli, G., Simoni, S., Bertoldi, W., Engel, M., Buter, A., Marchetti, G., Andreoli, A. & Comiti, F. (2022) Bedload Fluxes in a Glacier-Fed River at Multiple Temporal Scales. Water Resour. Res., 58, e2021WR031873. https://doi.org/10.1029/2021WR031873

635   Diplas, P., Dancey, C.L., Celik, A.O., Valyrakis, M., Greer, K. & Akar, T. (2008) The role of impulse on the initiation of particle movement under turbulent flow conditions. Science, 322(5902), 717–720.

Dwivedi, A., Melville, B.W., Shamseldin, A.Y. & Guha, T. (2010) Flow structures and sediment entrainment in a turbulent channel flow. J. Hydraul. Eng., 136(9), 623–632.

Elgueta-Astaburuaga, M.A., Hassan, M.A., Saletti, M. & Clarke, G.K.C. (2018) The effect of episodic sediment supply on
640   bedload variability and sediment mobility, Water Resour. Res., 54, 6319–6335, https://doi.org/10.1029/2017WR022280

Gaeuman, D., Andrews, E.D., Krause, A. & Smith, W. (2009) Predicting fractional bedload transport rates: Application of the Wilcock-Crowe equations to a regulated gravel-bed river, Water Resour. Res., 45, W06409. https://doi.org/10.1029/2008WR007320

Gaeuman, D., Holt, C.R. & Bunte, K. (2015) Maximum likelihood parameter estimation for fitting bedload rating curves,
645   Water Resour. Res., 51, 281–301.https://doi.org/10.1002/2014WR15872

Golly, A., Turowski, J.M., Badoux, A. & Hovius, N. (2017) Controls and feedbacks in the coupling of mountain channels and hillslopes, Geology, 45, 307–310, https://doi.org/10.1130/G38831.1

Gomez, B., Naff, R.L., & Hubbell, D.W. (1989) Temporal variations in bedload transport rates associated with the migration of bedforms. Earth Surf. Proc. Land., 14(2), 135–156.

650   Kreisler, A., Moser, M., Aigner, J., Rindler, R., Tritthart, M. & Habersack, H. (2017) Analysis and classification of bedload transport events with variable process characteristics. Geomorphology, 291, 57–68. Available from: https://doi.org/10.1016/j.geomorph.2016.06.033

Lisle, T.E., Iseya, F. & Ikeda, H. (1997) Response of a channel with alternate bars to a decrease in supply of mixed-size bed load: A flume experiment. Water Resour. Res., 33(8), 1971–1981.

655   Mao, L., Comiti, F., Carillo, R., Penna, D. (2019) Sediment Transport in Proglacial Rivers, in: Geomorphology of proglacial systems, Geography of the Physical Environment, 199–217, https://doi.org/10.1007/978-3-319-94184-4_12

Masteller, C.C. & Finnegan, N.J. (2017) Interplay between grain protrusion and sediment entrainment in an experimental flume. J. Geophys. Res.-Earth, 122, 274–289. https://doi.org/10.1002/2016JF003943

Masteller, C.C., Finnegan, N.J., Turowski, J.M., Yager, E.M. & Rickenmann, D. (2019) History-dependent threshold for
660   motion revealed by continuous bedload transport measurements in a steep mountain stream. Geophys. Res. Lett., 46, 2583–2591. https://doi.org/10.1029/2018GL081325

Meyer-Peter, E., & Müller, R. (1948) Formulas for bed-load transport. Proceedings of the 2nd Meeting, IAHR, 39–64.

Monsalve, A., Rickenmann, D., & Turowski, J.M. (2020) A bed load transport equation based on the spatial distribution of shear stress. Earth Surf. Dynam., 8(4), 825–847.

665   Nelson, J.M., Shreve, R.L., McLean, S.R. & Drake, T.G. (1995) Role of near-bed turbulence structure in bed load transport and bed form mechanics. Water Resour. Res., 31(8), 2071–2086.

Nicollier, T., Rickenmann, D. & Hartlieb, A. (2019) Field Calibration of the Swiss Plate Geophone System at the Albula Stream and Comparison with Controlled Flume Experiments. SedHyd2019, Federal Interagency Sedimentation and Hydrologic Modeling Conference. June 2019, Reno NV.
670   https://www.sedhyd.org/2019/openconf/modules/request.php?module=oc_program&action=program.php&p=program

Nicollier, T., Rickenmann, D., Boss., S, Travaglini, E. & Hartlieb, A. (2020) Calibration of the Swiss plate geophone system at the Zinal field site with direct bedload samples and results from controlled flume experiments. River Flow 2020, Uijttewaal et al. (eds), Taylor & Francis Group, London, ISBN 978-0-367-62773-7, pp. 901-909.

Nicollier, T., Rickenmann, D. & Hartlieb, A. (2021) Field and flume measurements with the impact plate: Effect of bedload
675   grain-size distribution on signal response. Earth Surf. Proc. Land.. 2021; 46:1504–1520. http://doi.org/10.1002/esp.5117

Nicollier, T., Antoniazza, G., Ammann, L., Rickenmann, D. & Kirchner, J.W. (2022) Toward a general calibration of the Swiss plate geophone system for fractional bedload transport. Earth Surf. Dynam., 10, 929-951, https://doi.org/10.5194/esurf-10-929-2022

Parker, G. (2008) Transport of gravel and sediment mixtures. In Sedimentation Engineering: Processes, Measurements,
680   Modeling, and Practice (pp. 165–252). ASCE.

Phillips, C.B. & Jerolmack, D.J. (2019) Bankfull transport capacity and the threshold of motion in coarse-grained rivers. Water Resour. Res., 55, https://doi.org/10.1029/2019WR025455

Pretzlav, K.L.G., Johnson, J.P.L. & Bradley, D.N. (2020) Smartrock transport in a mountain stream: Bedload hysteresis and changing thresholds of motion, Water Resour. Res., 56, e2020WR028150, https://doi.org/10.1029/2020WR028150

685 Recking, A. (2012) Influence of sediment supply on mountain streams bedload transport. Geomorphology, 175–176 (2012), 139–150, https://doi.org/10.1016/j.geomorph.2012.07.005

Recking, A. (2013) Simple method for calculating reach-averaged bed-load transport. Journal of Hydraulic Engineering, 139, 70–75, http://dx.doi.org/10.1061/(ASCE)HY.1943-7900.0000653

Recking A., Liébault F., Peteuil C., Jolimet T. (2012) Testing several bed load transport equations with consideration of time
690 scales. Earth Surf. Proc. Land., 37(7), 774–789, https://doi.org/10.1002/esp.3213

Recking, A., Piton, G., Vazquez-Tarrio, D. & Parker, G. (2016) Quantifying the morphological print of bedload transport. Earth Surf. Proc. Land., 41, 809–822, https://doi.org/10.1002/esp.3869

Rickenmann, D. (2017) Bed-load transport measurements with geophones and other passive acoustic methods. J. Hydraul. Eng., 60th Anniversary State-of-the-Art Reviews, 143(6), 03117004-1-14, doi: 10.1061/(ASCE)HY.1943-7900.0001300.

695 Rickenmann, D. (2018) Variability of bed load transport during six summers of continuous measurements in two Austrian mountain streams (Fischbach and Ruetz). Water Resour. Res., 54, 107–131. https://doi.org/10.1002/2017WR021376.

Rickenmann, D. (2020) Effect of sediment supply on cyclic fluctuations of the disequilibrium ratio and threshold transport discharge, inferred from bedload transport measurements over 27 years at the Swiss Erlenbach stream. Water Resour. Res., 56, e2020WR027741. https://doi.org/10.1029/2020WR027741

700 Rickenmann, D. (2024) Bedload transport fluctuations, flow conditions, and disequilibrium ratio at the Swiss Erlenbach stream: results from 27 years of high-resolution temporal measurements. Earth Surf. Dynam., 12, 11-34, https://doi.org/10.5194/esurf-12-11-2024

Rickenmann, D., Turowski, J.M., Fritschi, B., Klaiber, A. & Ludwig, A. (2012) Bedload transport measurements at the Erlenbach stream with geophones and automated basket samplers. Earth Surf. Proc. Land., 37, 1000-1011, doi:
705 10.1002/esp.3225.

Rickenmann, D., Antoniazza, G., Wyss, C.R., Fritschi, B. & Boss, S. (2017) Bedload transport monitoring with acoustic sensors in the Swiss Albula mountain river. Proc. IAHS, 375, 5-10, doi:10.5194/piahs-375-5-2017.

Rickenmann, D., Nicollier, T., Boss, S. & Badoux, A. (2020) Four years of bedload transport measurements in the Swiss mountain river Albula. River Flow 2020, Uijttewaal et al. (eds), Taylor & Francis Group, London, ISBN 978-0-367-62773-7,
710 pp. 1749-1755.

Rickenmann, D., Ammann, L., Nicollier, T., Boss, S., Fritschi, B., Antoniazza, G., Steeb, N., Chen, Z., Wyss, C. & Badoux, A. (2022) Comparison of calibration characteristics of different acoustic impact systems for measuring bedload transport in mountain streams. Earth Surf. Dynam., 10, 1165-1183, https://doi.org/10.5194/esurf-10-1165-2022

Rickenmann, D., Hug Peter, D., Ammann, L., Nicollier, T. & Badoux, A. (2024) Indirekte Geschiebetransportmessung, Teil
715 2: Fraktionierter Transport, Unsicherheiten, Perspektiven. Wasser, Energie, Luft, 116(2), 111-119.

Rickenmann, D., Hug Peter, D., Ammann, L., Nicollier, T., Boss, S., Fritschi, B., Wyss, C., Antoniazza, G. & Badoux, A. (2024) Surrogate bedload measurements in mountain rivers: system comparison, uncertainty, new prototype. Preliminary version: Conference Proceedings INTERPRAEVENT 2024, 685-689

Rindler, R., Schwarz, S., Lammer, A., Shire-Peterlechner, D., Gmeiner, P., Liedermann, M. et al. (2025) From glaciers to large rivers: Lessons and insights from long-term bedload monitoring. Earth Surf. Proc. Land., 50(5), e70059. https://doi.org/10.1002/esp.70059

Schmeeckle, M.W., & Nelson, J.M. (2003) Direct numerical simulation of bedload transport using a local, dynamic boundary condition. Sedimentology, 50(2), 279–301.

Schneider, J.M., Rickenmann, D., Turowski, J.M., Bunte, K. & Kirchner, J.W. (2015a) Applicability of bedload transport models for mixed-size sediments in steep streams considering macro-roughness. Water Resour. Res., 51, 5260–5283, https://doi.org/10.1002/2014WR016417

Schneider, J.M., Rickenmann, D., Turowski, J.M. & Kirchner, J.W. (2015b) Self-adjustment of stream bed roughness and flow velocity in a steep mountain channel. Water Resour. Res., 51, 7838–7859, doi:10.1002/ 2015WR016934

Schneider, J.M., Rickenmann, D., Turowski, J.M., Schmid, B. & Kirchner, J.W. (2016) Bed load transport in a very steep mountain stream (Riedbach, Switzerland): Measurement and prediction. Water Resour. Res., 52, 9522–9541, doi:10.1002/2016WR019308

Turowski, J. M., Yager, E. M., Badoux, A., Rickenmann, D., and Molnar, P. (2009) The impact of exceptional events on erosion, bedload transport and channel stability in a step-pool channel, Earth Surf. Proc. Land., 34, 1661–1673, https://doi.org/10.1002/esp.1855

Valyrakis, M., Diplas, P., Dancey, C.L., Greer, K., & Celik, A. O. (2010) Role of instantaneous force magnitude and duration on particle entrainment. J. Geophys. Res.-Earth, 115(F2).

Vázquez-Tarrío, D., Piégay, H., Menéndez-Duarte, R.: Textural signatures of sediment supply in gravel-bed rivers: Revisiting the armour ratio. Earth-Sci. Rev., 207, 2020, 103211, https://doi.org/10.1016/j.earscirev.2020.103211

Villaret, C., Hervouet, J.M., Kopmann, R., Merkel, U., Davies, A.G. (2013). Morphodynamic modeling using the Telemac finite-element system. Comput. Geosci., 53, 105-113, https://doi.org/10.1016/j.cageo.2011.10.004

Warburton, J. (1992) Observations of bed load transport and channel bed changes in a proglacial mountain stream, Arctic Alpine Res., 24, 195–203.

Wilcock, P.R. and Crowe, J.C. (2003) Surface-based transport model for mixed-size sediment, J. Hydraul. Eng., 129, 120–128, https://doi.org/10.1061/(ASCE)0733-9429(2003)129:2(120)

Wilcock, P.R., & McArdell, B. W. (1993) Surface-based fractional transport rates: Mobilization thresholds and partial transport of a sand–gravel sediment. Water Resour. Res., 29(4), 1297–1312.

Yavuz, V.S. (2025). Calculation sedimentation by sediment modelling using HEC-RAS. In River Flow 2024, pp. 698-706. CRC Press.